IRREGULAR POLLEN EXINE1 Is a Novel Factor in Anther Cuticle and Pollen Exine Formation[1][OPEN]

Xiaoyang Chen[2], Hua Zhang[2,3], Huayue Sun[2], Hongbing Luo, Li Zhao, Zhaobin Dong, Shuangshuang Yan, Cheng Zhao, Renyi Liu, Chunyan Xu, Song Li, Huabang Chen*, and Weiwei Jin*

National Maize Improvement Center of China, Beijing Key Laboratory of Crop Genetic Improvement, MOE Key Laboratory of Crop Heterosis and Utilization (X.C., H.S., Z.D., W.J.), and Department of Vegetable Sciences, Beijing Key Laboratory of Growth and Developmental Regulation for Protected Vegetable Crops (S.Y.), China Agricultural University, Beijing 100193, China; State Key Laboratory of Plant Cell and Chromosome Engineering, Institute of Genetics and Developmental Biology, Chinese Academy of Sciences, Beijing 100101, China (H.Z., L.Z., C.X., S.L., H.C.); College of Agronomy, Southern Regional Collaborative Innovation Center for Grain and Oil Crops, Hunan Agricultural University, Changsha, Hunan 410128, China (H.L.); Shanghai Center for Plant Stress Biology, Shanghai Institute for Biological Sciences, Chinese Academy of Sciences, Shanghai 201602, China (C.Z., R.L.); and University of the Chinese Academy of Sciences, Beijing 100039, China (H.Z.)

ORCID IDs: 0000-0002-4656-3189 (H.S.); 0000-0003-0518-5924 (C.Z.); 0000-0001-9320-9628 (W.J.).

Anther cuticle and pollen exine are protective barriers for pollen development and fertilization. Despite that several regulators have been identified for anther cuticle and pollen exine development in rice (*Oryza sativa*) and Arabidopsis (*Arabidopsis thaliana*), few genes have been characterized in maize (*Zea mays*) and the underlying regulatory mechanism remains elusive. Here, we report a novel male-sterile mutant in maize, *irregular pollen exine1* (*ipe1*), which exhibited a glossy outer anther surface, abnormal Ubisch bodies, and defective pollen exine. Using map-based cloning, the *IPE1* gene was isolated as a putative glucose-methanol-choline oxidoreductase targeted to the endoplasmic reticulum. Transcripts of *IPE1* were preferentially accumulated in the tapetum during the tetrad and early uninucleate microspore stage. A biochemical assay indicated that *ipe1* anthers had altered constituents of wax and a significant reduction of cutin monomers and fatty acids. RNA sequencing data revealed that genes implicated in wax and flavonoid metabolism, fatty acid synthesis, and elongation were differentially expressed in *ipe1* mutant anthers. In addition, the analysis of transfer DNA insertional lines of the orthologous gene in Arabidopsis suggested that IPE1 and their orthologs have a partially conserved function in male organ development. Our results showed that IPE1 participates in the putative oxidative pathway of C16/C18 ω-hydroxy fatty acids and controls anther cuticle and pollen exine development together with MALE STERILITY26 and MALE STERILITY45 in maize.

Male sterility is a common biological phenomenon in plants and widely used in the production of hybrid seeds, which can reduce costs and enhance seed purity (Tester and Langridge, 2010). According to inheritance or origin, male sterility includes three types: genic male sterility, cytoplasmic male sterility, and cytoplasmic-genic male sterility (Rhee et al., 2015). The generation of mature pollen grains relies on anther development. The start of anther formation occurs in differentiated flower tissues (floral meristem), which consist of three histogenic layers: L1, L2, and L3. After continuous cell division and differentiation, L1 forms the epidermis and the L3 layer develops into the stomium and vascular bundles. L2 is the most important layer; it undergoes a series of periclinal and anticlinal divisions and eventually grows into the endothecium, the middle layer, the tapetum, and the pollen mother cells. When anther morphogenesis is completed, the anther has centrally localized pollen mother cells enclosed by four somatic layers, which are, from the surface to the interior, the epidermis, endothecium, middle layer, and tapetum. Then, the pollen mother cells undergo meiosis and mitosis, resulting in trinucleate pollen grains, and the endothecium, middle layer, and tapetum are gradually degraded (Goldberg et al., 1993, 1995; Ma, 2005).

The anther cuticle and pollen exine are two barriers for anther development and fertilization. However, their chemical nature is obscure because of the limitation of purifying and obtaining a sufficient quantity of materials for analysis. Previous results indicate that the anther cuticle, covering the outer surface of anthers, contains cutin and wax. The polymerization of hydroxylated and epoxy C16 and C18 fatty acids produces cutin (Pollard et al., 2008; Beisson et al., 2012), and a mixture of very-long-chain fatty acids, alkanes, alkenes, and fatty alcohols forms wax (Samuels et al., 2008). Pollen exine, occurring on the outer surface of pollen, consists of two sublayers, the sexine and nexine. Sexine is further divided into bacula and tectum. The major component of pollen exine is the very insoluble sporopollenin, which may be made of aliphatic derivatives such as fatty acids and phenolic compounds (Ariizumi and Toriyama, 2011). The innermost of the anther wall, the tapetum, has been considered the place where

nutrients and enzymes are synthesized (Stieglitz, 1977; Ariizumi and Toriyama, 2011). These materials can be transferred to the surface of anthers and pollen with the help of transporters and the specialized structures called Ubish bodies (Wang et al., 2003). Until now, several genes have been discovered in rice (*Oryza sativa*) that are involved in the development of the anther cuticle and pollen wall, including *WAX-DEFICIENT ANTHER1* (*WDA1*; Jung et al., 2006), *CYP704B2* (Li et al., 2010), *DEFECTIVE POLLEN WALL* (*DPW*; Shi et al., 2011), *CYP703A3* (Yang et al., 2014), *POSTMEIOTIC DEFICIENT ANTHER1* (Hu et al., 2010; Zhu et al., 2013), *OsABCG15* (Niu et al., 2013; Qin et al., 2013), *OsABCG26* (Zhao et al., 2015), and *TAPETUM DEGENERATION RETARDATION* (*TDR*; Li et al., 2006). Nevertheless, their regulatory networks still need to be explored.

With advances of forward and reverse genetics, some male-sterile genes have been isolated in maize, such as *MALE STERILE CONVERTED ANTHER1* (Chaubal et al., 2003), *MULTIPLE ARCHESPORIAL CELLS1* (Wang et al., 2012), *MALE STERILITY32* (*MS32*; Moon et al., 2013), *MS8* (Wang et al., 2013), *AMEIOTIC1* (Pawlowski et al., 2009), *ABSENCE OF FIRST DIVISION1* (Golubovskaya et al., 2006), *RECOMBINATION PROTEIN51* (Li et al., 2007), *MS26* (Albertsen et al., 2006), and *MS45* (Albertsen et al., 1993). Only *MS26* and *MS45* are required for pollen wall development, but their detailed functions have not been confirmed. *MS45* may encode a strictosidine synthase, which is localized in the tapetum during the early vacuolization stage of microspore development (Cigan et al., 2001; Skibbe and Schnable, 2005). In the *ms26* mutant, tapetal cells degenerate abnormally. Microspores show early vacuolation and are aborted after the tetrad stage. *MS26* probably encodes a cytochrome P450 monooxygenase (Djukanovic et al., 2013) that is homologous to *CYP704B1* in Arabidopsis (*Arabidopsis thaliana*), *CYP704B2* in rice, and *BnMS1* and *BnMS2* in *Brassica napus*, the mutation of which results in defective pollen exine. CYP704B1 and CYP704B2 have a similar function in the ω-hydroxylation of C16 and C18 fatty acids (Dobritsa et al., 2009; Li et al., 2010; Yi et al., 2010). The mechanism of anther cuticle and pollen wall development remains largely unknown in maize.

In this study, we obtained a complete maize male-sterile mutant, *irregular pollen exine1* (*ipe1*), which had a smooth outer anther surface, defective Ubisch bodies, abnormal pollen exine, and no mature pollen grains. Through position cloning and transgenic experiments, we cloned the *IPE1* gene as a putative Glc-methanol-choline (GMC) oxidoreductase that was expressed mainly in the tapetum. The expression of IPE1 fused with GFP indicated that IPE1 was localized in the endoplasmic reticulum by the N-terminal signal peptide. A remarkably altered composition of cutin, wax, and fatty acids was observed in the *ipe1* mutant. Moreover, the expression of wax and flavonoid metabolism genes, and fatty acid synthesis and elongation genes, was changed in *ipe1* anthers. Our data indicated that the putative oxidative pathway of ω-hydroxy fatty acids depending on IPE1 plays an important role in anther cuticle and pollen exine formation in maize.

RESULTS

Isolation and Phenotypic Analysis of the *ipe1* Mutant

To identify more male-sterile genes in maize, we screened a MuDR library (Dong et al., 2013) and obtained the complete male-sterile mutant *ipe1*. When crossed with the wild type, all F1 progeny were fertile, with the F2 population segregating at an approximate ratio of 3:1 (fertility:sterility = 208:58, $\chi^2 < \chi^2_{(0.05,\ 1)} = 3.84$), indicating that the mutant phenotype was controlled by a single recessive gene. Compared with the wild type, there were no obvious differences in *ipe1* during vegetative growth (Fig. 1, A and B). However, the mutant anthers could not be spread from glumes (Fig. 1, C and D) and became smaller, wilted, and brown with no mature pollen grains (Fig. 1, E–H). *ipe1* plants could normally set seeds when pollinated with wild-type pollen, implying that female fertility was unaffected.

Anther Development Was Defective in the *ipe1* Mutant

To check the defect of *ipe1* during anther development, we first analyzed microspore development in the wild type and *ipe1* by 4′,6-diamidino-2-phenylindole (DAPI) staining. Normal meiosis and tetrads were observed in the *ipe1* mutant (Fig. 2, A and F; Supplemental Fig. S1). At the early uninucleate microspore stage, similar to that in the wild type, *ipe1* microspores were normally released from the tetrad and the nucleus was located in the middle (Fig. 2, B and G). At the following

[1] This work was supported by the National Natural Science Foundation of China (grant nos. 31471499, 31271729, 91535206, and 31421005), the National Key Research and Development Program of China (grant no. 2016YFD0101201), and the Ministry of Agriculture of China (grant no. 2016ZX08009003–003).

[2] These authors contributed equally to the article.

[3] Present address: National Engineering Laboratory of Wheat and Maize, Maize Research Institute, Shandong Academy of Agricultural Sciences, Ji'nan, Shandong 250100, China.

* Address correspondence to hbchen@genetics.ac.cn and weiweijin@cau.edu.cn.

The author responsible for distribution of materials integral to the findings presented in this article in accordance with the policy described in the Instructions for Authors (www.plantphysiol.org) is: Weiwei Jin (weiweijin@cau.edu.cn).

X.C., H.Z., H.S., and Z.D. performed phenotypic analysis, mapped and cloned *IPE1*, carried out expression analysis, and wrote the article; H.Z., C.X., S.L., and L.Z. conducted anther wax, cutin, and fatty acid assays, transgene experiments, and subcellular localization; H.L. provided *ipe1* and *ipe1-2* mutants; S.Y. performed RNA in situ hybridizations; C.Z. and R.L. analyzed the RNA-Seq data; W.J. and H.C. helped design the research and edited the article.

[OPEN] Articles can be viewed without a subscription.

www.plantphysiol.org/cgi/doi/10.1104/pp.16.00629

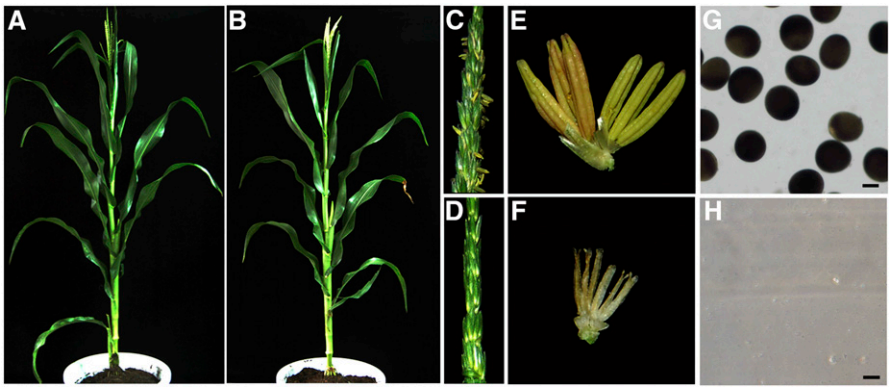

Figure 1. Morphological comparisons between the wild type and *ipe1*. A and B, No significant difference was observed between the wild type (A) and *ipe1* (B) at the tasseling stage. C and D, Mutant anthers (D) are hidden in the glume compared with wild-type anthers (C) after flowering. E and F, In the wild type, six anthers are filled and dark yellow (E), whereas *ipe1* anthers are wilted, smaller, and brown (F). G and H, At the mature pollen grain stage, by staining with 1% odine-potassium iodide (I_2-KI) solution, abundant mature pollen grains are present in wild-type anthers (G) but completely absent in *ipe1* mutant anthers (H). Bars = 50 μm.

stages, in the wild type, the size of microspores increased gradually and the pollen wall was formed; the nucleus moved to the peripheral region and then underwent mitosis to generate two nuclei: a generative nucleus and a vegetative nucleus (Fig. 2, C–E). However, the pollen wall of *ipe1* was undeveloped, which resulted in microspores slowly collapsing and aborting (Fig. 2, H and I). Eventually, only some remnant material was left at the binucleate microspore stage (Fig. 2J), implying that defects of the *ipe1* microspore start with pollen wall formation after the tetrad stage.

Furthermore, a transverse section was made for more detailed characterization of the *ipe1* defect. At the tetrad stage, like the wild-type anther, four anther wall layers persisted, surrounding the tetrad in *ipe1* (Fig. 2, K and P). At the early uninucleate microspore stage, in wild-type anthers, there was the thin middle layer and the tapetum was degraded and appeared more condensed and deeply stained (Fig. 2L). However, the *ipe1* middle layer could not be seen, and tapetal cells were lightly stained. More vacuoles appeared in the tapetum than in the wild type, suggesting more severe degradation of the tapetum. Microspores could be released normally from the tetrad with a natural shape (Fig. 2Q). During the late uninucleate microspore stage, the middle layer of wild-type anthers disappeared and the tapetum continued to be degraded. Microspores became vacuolated and gradually enlarged, and the pollen exine was clearly visible and became darker, suggesting that more sporopollenin precursors had been deposited on the surface of microspores (Fig. 2M). By contrast, in *ipe1* anthers, the tapetum was almost completely degraded and less cellular material was left. Microspores appeared to be degraded and exhibited an irregular appearance, and the pollen exine could not be observed distinctly (Fig. 2R). At the binucleate microspore stage, the wild-type tapetum displayed a strip shape and vacuolated microspores showed the falcate form (Fig. 2N). Unlike the wild type, the *ipe1* microspores and anther wall had collapsed (Fig. 2S). At the mature pollen grain stage, many pollen grains were observed in the anther locule of the wild type (Fig. 2O). On the contrary, in *ipe1* anthers, no pollen grains existed and only some debris remained (Fig. 2T). These phenotypes confirmed that *IPE1* is involved in the degeneration of the tapetum in anther development.

Scanning electron microscopy (SEM) was used to investigate anther development at the mature pollen grain stage. Consistent with the above morphological results, *ipe1* anthers produced smaller, wilted anthers with no pollen grains in the anther locule (Fig. 3, A–E). Moreover, reticulate cuticle coated the outermost surface of anthers, and abundant Ubisch bodies were distributed on the outside of tapetal cells in wild-type anthers (Fig. 3, F and H). However, the *ipe1* anther surface was smooth (Fig. 3G), indicating that anther cuticle formation was disrupted in the mutant. In addition, Ubisch bodies could not be seen on the inner surface of mutant anthers (Fig. 3I).

To further examine the *ipe1* defects, transmission electron microscopy (TEM) was employed. According to DAPI staining and transverse sectioning, no apparent differences were detected at the tetrad stage between the wild type and *ipe1* (Fig. 4, A–D). At the early uninucleate microspore stage, tapetal cells of the wild type contained numerous subcellular organelles (Fig. 4, E and G). In the *ipe1* tapetal cells, the Ubisch bodies were normally obvious, as in the wild type (Fig. 4, I and J). However, fewer subcellular organelles and lipid bodies but more vacuoles were observed, which indicated that lipid metabolism was influenced (Fig. 4, F and H). At this stage, microspores of the wild type had begun to form the exine, consisting of bacula and nexine (Fig. 4, K and M). By contrast, *ipe1* microspores did not develop the dark bacula structure (Fig. 4, L and N). During the late uninucleate microspore stage, the wild-type

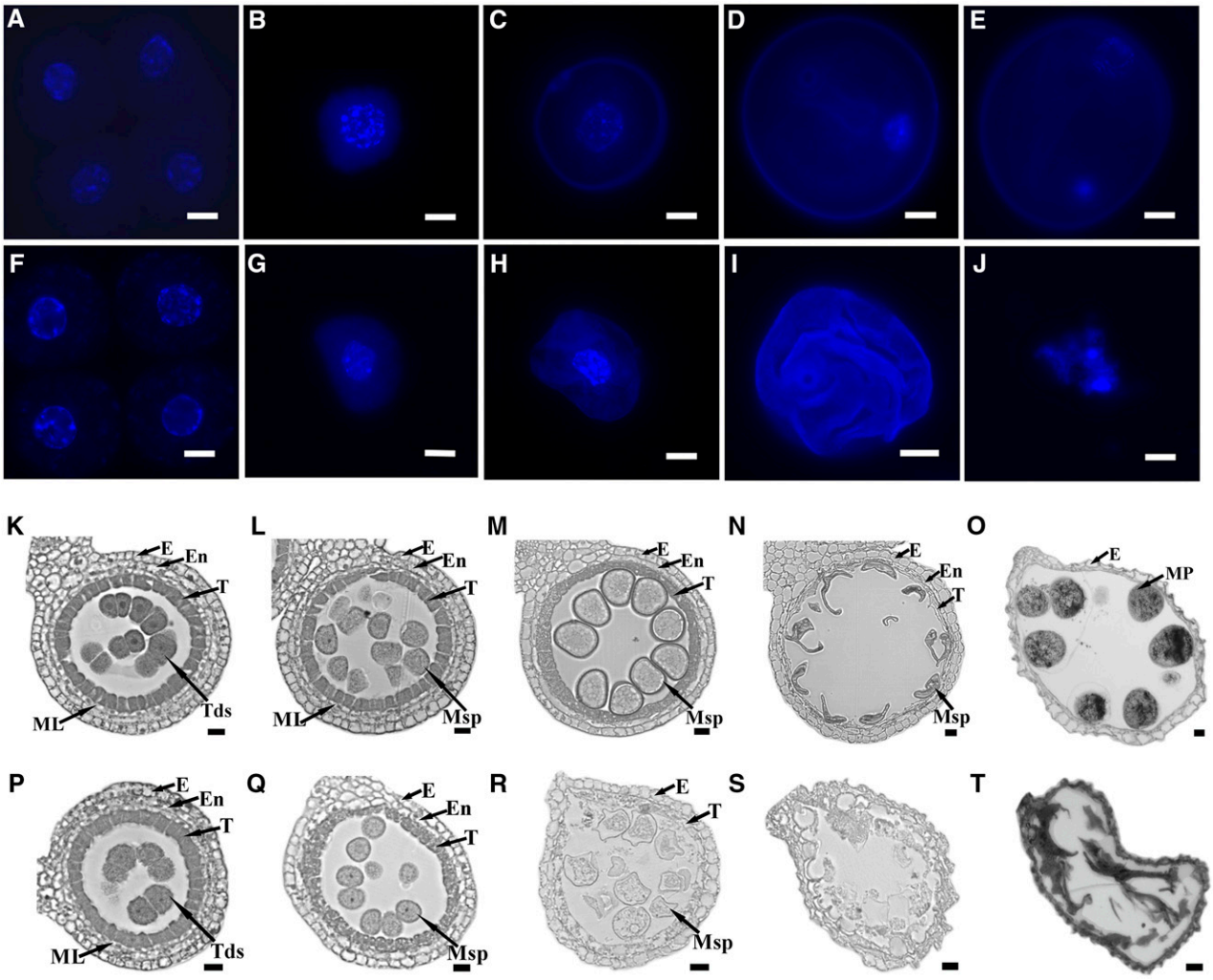

Figure 2. Phenotypic analysis of *ipe1* anthers at various developmental stages. A to J, DAPI staining of wild-type (A–E) and *ipe1* (F–J) microspores. A and F, At the tetrad stage, the normal tetrad is shown in the wild type (A) and mutant (F). B and G, At the early uninucleate stage, normal microspores of the wild type (B) and mutant (G) are free from the tetrad. C and H, At the middle uninucleate stage, the pollen wall of wild-type microspores is distinct (C), while the shape of the microspore is irregular and the pollen wall is not well formed in the mutant (H). D and I, At the late uninucleate stage, compared with the wild-type microspore (D), the *ipe1* microspore is severely disorganized (I). E and J, At the binucleate stage, in the wild type (E), the larger microspore has a vegetative nucleus and a generative nucleus, while the *ipe1* microspore is completely degenerated (J). Bars = 10 μm. K to T, Transverse sections of wild-type and *ipe1* anthers. A single locule is shown from cross sections of the wild type (K–O) and the *ipe1* mutant (P–T). K and P, At the tetrad stage, both the wild-type (K) and mutant (P) anthers with four somatic layers and tetrads are shown. L and Q, At the early uninucleate stage, the tapetum is condensed and deeply stained in the wild type (L). While the *ipe1* middle layer is missing, the tapetum is lightly stained with more vacuoles present (Q). M and R, At the late uninucleate stage, the *ipe1* tapetum is almost completely degraded and microspores degenerated without the dark pollen exine (R) compared with the wild type (M). N and S, At the binucleate stage, in the mutant (S), collapsed anther layers and microspores are observed compared with the wild type (N). O and T, At the mature pollen grain stage, no mature pollen grains are found in the mutant (T) compared with the wild type (O). E, Epidermis; En, endothecium; ML, middle layer; MP, mature pollen; Msp, microspore; T, tapetum; Tds, tetrads. Bars = 20 μm.

tapetum degenerated but parts of subcellular organelles existed (Fig. 4, O and Q). Ubisch bodies accumulated enough sporopollenin precursors (Fig. 4S). However, the *ipe1* tapetum had been degraded completely and barely functional Ubisch bodies could be observed (Fig. 4, P, R, and T). Meanwhile, wild-type microspores formed a thicker pollen exine that consisted of tectum, bacula, and nexine (Fig. 4, U and W). In contrast, sporopollenin precursors were distributed randomly and the pollen exine did not have the typical three-layer structure in *ipe1* (Fig. 4, V and X). These observations illustrated that IPE1 functions in the formation of the anther cuticle, Ubisch bodies, and pollen exine.

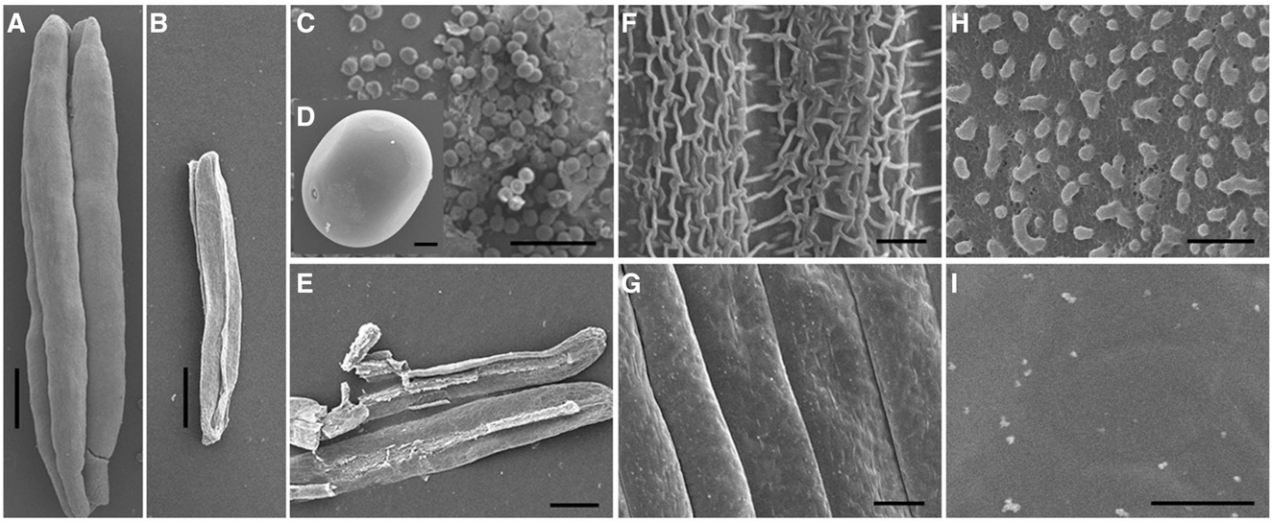

Figure 3. SEM analysis of wild-type and *ipe1* anthers at the mature pollen grain stage. A and B, The *ipe1* anther (B) is smaller and wilted than the normal anther (A). C to E, Abundant mature pollen grains are observed in the wild type (C) but have vanished in the mutant (E). A wild-type pollen grain is shown in D. F to I, The outer (F) and inner (H) surfaces of wild-type anther compared with the outer (G) and inner (I) surfaces of *ipe1* anther. The *ipe1* anther outer surface is glossy with no Ubisch bodies on the inner anther surface. Bars = 600 μm in A and B, 400 μm in C and E, 15 μm in D, 6 μm in F and G, and 2 μm in H and I.

Alteration of Wax, Cutin, and Fatty Acids in *ipe1* Anther

The phenotypic defects of the anther cuticle, pollen wall, and Ubisch bodies in *ipe1* revealed that abnormalities may occur in the synthesis or transport of aliphatic compounds. To test this hypothesis, we used gas chromatography-mass spectrometry (GC-MS) to determine the constituents of chloroform-extractable cuticular waxes, cutin, and fatty acids in wild-type and *ipe1* anthers. We calculated the surface areas of randomly chosen anthers and then plotted them against the weight of each sample to determine the surface areas of corresponding samples (Li et al., 2010; Shi et al., 2011; Supplemental Fig. S2).

Our results showed that there was no significant variation in the total wax between *ipe1* anthers (21.17 ng mm^{-2}) and wild-type anthers (17.37 ng mm^{-2}; $P > 0.05$). By contrast, the total cutin of *ipe1* anthers (130.91 ng mm^{-2}) decreased by 78.25% compared with the wild type (601.79 ng mm^{-2}; $P < 0.01$; Fig. 5A). For the wax constituents, C23, C25, C27, C29, and C31 alkanes were increased significantly in *ipe1* ($P < 0.01$) while C33 and C35 alkanes were obviously decreased ($P < 0.01$; Fig. 5B). In addition, significant increases in the levels of C24, C26, C28, C30, and C32 alcohols ($P < 0.05$) were detected in mutant anthers (Fig. 5B). In the wild-type anther, the major aliphatic cutin monomers were C16:0, C18:2, C18:3, C16:0 ω-OH, C18:1 ω-OH, C18:2 ω-OH, C18:0 9/10 di-OH, and C18:0 tri-OH acids (Fig. 5C). Compared with the wild type, all aliphatic cutin monomers observed in the *ipe1* anthers were reduced significantly (Fig. 5C; Supplemental Table S1). Fatty alcohols, alkanes, and other aliphatic molecules are derivatives of fatty acids (Zhang et al., 2008). To understand the alteration of the levels of fatty acids, the total fatty acids of anthers were extracted for analysis. The level of total fatty acids of wild-type anthers with carbon length from C14 to C28 was 61.51 μg mg^{-1}, whereas that of *ipe1* anthers was only 32.15 μg mg^{-1} (Table I). Chemical analysis indicated that *IPE1* participates in lipidic metabolism or transport necessary for anther development.

Map-Based Cloning of *IPE1*

We used the map-based cloning approach to isolate the responsible gene for the *ipe1* mutant. The *IPE1* gene was initially mapped on the chromosome 1 short arm between simple sequence repeat markers S1 and S11 (Fig. 6A). We then developed nine pairs of insertion-deletion (Indel) markers for fine mapping (Supplemental Table S2). Using 4,021 mutant individuals from the F2 population, the target genomic region was ultimately narrowed to the approximately 290-kb interval between Indel markers S4 and S8, with nine and 11 recombination individuals, respectively (Fig. 6A). Six predicted genes were located in this interval (Fig. 6A), and one of these genes, *GRMZM2G434500*, was identified to have a Mutator1 transposon (Mu1) insertion at the 64th base pair from the beginning of the third exon by sequencing the *ipe1* genomic DNA (Fig. 6B).

In addition, we obtained three other male-sterile lines, named *ipe1-1* (*mu1019442*::*Mu*), *ipe1-2*, and *ipe1-3* (*ms*-6044*). They all exhibited a smooth anther surface, which was very similar to the *ipe1* phenotype (Supplemental Fig. S3). Allelism tests confirmed that *ipe1-1*, *ipe1-2*, and *ipe1-3* were all allelic to

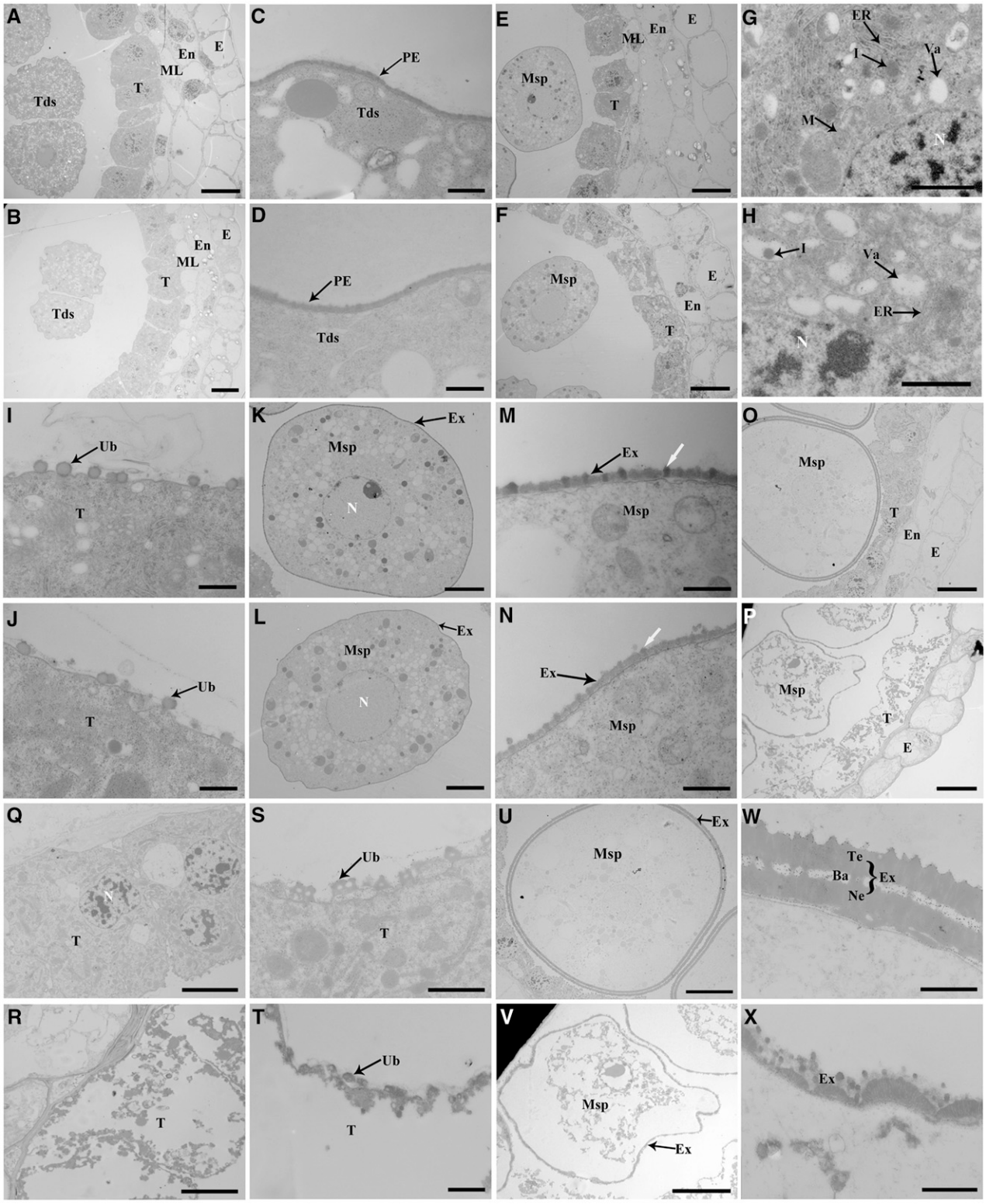

Figure 4. TEM of anthers in the wild type and the *ipe1* mutant. A and B, Normal anthers of the wild type (A) and the mutant (B) are shown at the tetrad stage. C and D, On the surface of the microspore, the primexine is normally developed in the wild type (C) and the mutant (D) at the tetrad stage. E and F, Anthers of the wild type (E) and the mutant (F) show the defective *ipe1* tapetum with light staining at the early uninucleate microspore stage. G, Higher magnification of the wild-type tapetum in E shows abundant subcellular organelles. H, Higher magnification of the *ipe1* tapetum in F shows fewer subcellular organelles. I and J, Normal Ubisch bodies of the wild type (I) and the mutant (J) are shown at the early uninucleate microspore stage. K and L, The shape of

ipe1 (Supplemental Table S3). Sequencing of the *GRMZM2G434500* gene in these mutants revealed the mutated sites: there was a Mu3 transposon insertion at the 49th base pair from the starting nucleotide of translation in *ipe1-1*, a deletion containing the entire GRMZM2G434500 in *ipe1-2*, and a 1,331-bp insertion at the 691st base pair from the beginning of the third exon in *ipe1-3* (Fig. 6B), verifying that *GRMZM2G434500* was responsible for the male-sterile phenotype in *ipe1*. The *IPE1* gene was further confirmed by functional complementation of *ipe1-3* homozygous plants and targeted gene knockouts of *IPE1* by the CRISPR-Cas9 system (Fig. 6, C–P).

Sequence analysis of cDNA confirmed that the *IPE1* gene consisted of three exons and two introns (Fig. 6B) and encoded a 582-amino acid protein. Structure prediction using SMART (http://smart.embl-heidelberg.de/) indicated that IPE1 included two domains of the GMC oxidoreductase at the N terminus (50–323) and C terminus (424–571; Fig. 6Q). Further analysis by National Center for Biotechnology Information BLAST revealed that IPE1 was a putative GMC oxidoreductase.

Partially Functional Conservation of the *IPE1* Orthologous Gene in Arabidopsis

To demonstrate whether the function of *IPE1* in anther cuticle and pollen exine development is conserved, we constructed a phylogenetic tree based on IPE1 and 17 of the most similar protein sequences from maize, rice, and Arabidopsis (Supplemental Fig. S4). Most of these genes have a common GMC domain and are highly expressed in the male reproductive organs (Supplemental Fig. S5; Supplemental Table S4), indicating that they may have a conserved function in the formation of the male reproductive organs. The phylogenetic tree suggested that the *AT1G12570* gene was the most closely orthologous gene for *IPE1* in Arabidopsis. To address the function of *AT1G12570*, we obtained a T-DNA line (SALK-085330C) with an insertion in the fourth exon (Fig. 7A), resulting in premature transcription termination (Fig. 7B). Compared with the wild type, the T-DNA line had the normal pollen-grain extrusion and anther cuticle development (Fig. 7, C–F). However, pollen grains that were smaller than wild-type ones were detected and the percentage of mutant pollen grains was about 23% (293 of 1,272; Fig. 7, G–I). Moreover, the surface of some pollen grains with normal size was smooth to varying degrees (Fig. 7, J and K). Two allelic mutants (SALK-112758 and SALK-031400) of *AT1G12570* showed similar phenotypes to the mutant (Supplemental Fig. S6), indicating that *AT1G12570* is involved in pollen grain maturation and pollen exine development but not in anther cuticle development. These data suggested that the Arabidopsis ortholog of *IPE1* plays a partially conserved role in anther development.

IPE1 Is Expressed Predominantly in the Tapetum

According to phenotypic analysis, the formation of anther cuticle and pollen exine was abnormal in *ipe1* anthers, while there was no obvious mutant phenotype in vegetative growth. To examine whether the expression and function of *IPE1* are consistent, the expression pattern of *IPE1* was evaluated. Total RNA extracted from vegetative and reproductive organs was used to perform RT-PCR. The *IPE1* transcript was detected in young spikelets with no apparent detection in roots, stems, leaves, glumes, cobs, and pistils, which agreed with the mutant phenotype (Fig. 8A). Anthers at different developmental stages were collected to further determine the expression pattern. *IPE1* was expressed specifically at the early uninucleate microspore stage (Fig. 8B), which was confirmed by quantitative reverse transcription (qRT)-PCR (Fig. 8C). However, no evident expression was detected at the meiosis stage, late uninucleate microspore stage, binucleate microspore stage, and mature pollen grain stage (Fig. 8B).

To accurately determine the spatial and temporal expression of *IPE1*, we employed RNA in situ hybridization with wild-type anthers at various stages. Consistent with the RT-PCR results, *IPE1* was strongly and predominantly expressed in the tapetum at the tetrad stage and early uninucleate stage (Fig. 8, F and G), and

Figure 4. (*Continued.*)
microspores is normal in the wild type (K) and the mutant (L) at the early uninucleate microspore stage. M and N, The pollen exine of the wild type (M) and the mutant (N) shows the primary structure of the pollen exine; the dark bacula (white arrows) are not clearly visible in the *ipe1* microspore at the early uninucleate microspore stage. O and P, Anthers of the wild type (O) and the mutant (P) show the defects of *ipe1* anthers with abnormal tapetum and microspores at the late uninucleate microspore stage. Q, Higher magnification of the wild-type tapetum in O shows that a portion of subcellular organelles are present in the degenerated tapetum. R, Higher magnification of the mutant tapetum in P shows that the *ipe1* tapetum is almost completely degraded with only remnants remaining. S and T, Ubisch bodies have accumulated abundant electron-dense sporopollenin precursors in the wild type (S), while *ipe1* Ubisch bodies are severely degenerated and have almost disappeared (T) at the late uninucleate microspore stage. U and V, Microspores of the wild type (U) and the mutant (V) show the disordered microspore of *ipe1* at the late uninucleate microspore stage. W and X, The wild-type pollen exine contains tectum, bacula, and nexine (W), while in the *ipe1* mutant, the structure of pollen exine is not intact (X) at the late uninucleate microspore stage. Ba, Bacula; E, epidermis; En, endothecium; ER, endoplasmic reticulum; Ex, exine; l, lipid body; M, mitochondria; ML, middle layer; Msp, microspore; N, nucleus; Ne, nexine; PE, primexine; T, tapetum; Tds, tetrads; Te, tectum; Ub, Ubisch body; Va, vacuole. Bars = 10 μm in A, B, E, F, O, P, U, and V, 5 μm in K, J, Q, and R, 1 μm in G and H, 1 μm in S, T, W, and X, and 0.5 μm in C, D, I, J, M, and N.

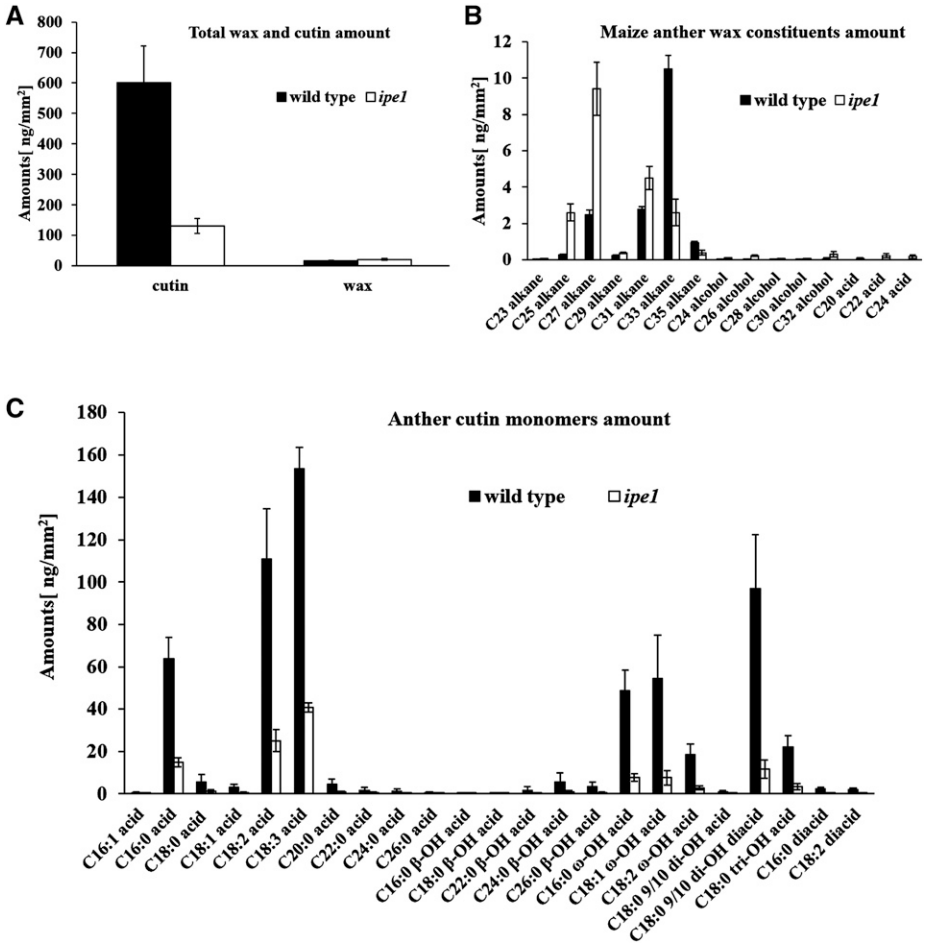

Figure 5. Analysis of anther wax and cutin in the wild type and the *ipe1* mutant. A, Total cutin and wax amounts per unit of surface area (ng mm^{-2}) in wild-type (black bars) and *ipe1* (white bars) anthers. Error bars indicate SD ($n = 5$). B, Wax constituent amounts per unit of surface area (ng mm^{-2}) in wild-type (black bars) and *ipe1* (white bars) anthers. Error bars indicate SD ($n = 5$). C, Cutin constituent amounts per unit of surface area (ng mm^{-2}) in wild-type (black bars) and *ipe1* (white bars) anthers. Error bars indicate SD ($n = 5$). Compound names are abbreviated as follows: C16:1 acid, 7-hexadecenoic acid; C16:0 acid, hexadecanoic acid; C18:0 acid, octadecanoic acid; C18:1 acid, oleic acid; C18:2 acid, linoleic acid; C18:3 acid, linolenic acid; C20:0 acid, eicosanoic acid; C22:0 acid, docosanoic acid; C24:0 acid, tetracosanoic acid; C26:0 acid, hexacosanoic acid; C16:0 β-OH acid, 2-hydroxy-hexadecanoic acid; C18:0 β-OH acid, 2-hydroxy-octadecanoic acid; C22:0 β-OH acid, 2-hydroxy-docosanoic acid; C24:0 β-OH acid, 2-hydroxy-tetracosanoic acid; C26:0 β-OH acid, 2-hydroxy-hexacosanoic acid; C16:0 ω-OH acid, 16-hydroxy-hexadecanoic acid; C18:1 ω-OH acid, 18-hydroxy-oleic acid; C18:2 ω-OH acid, 18-hydroxy-linoleic acid; C18:0 9/10 di-OH acid, 9,10-dihydroxy-octadecanoic acid; C18:0 9/10 di-OH diacid, 9,10-dihydroxy-octadecanoic-1,18-dioic acid; C18:0 tri-OH acid, 9,10,18-trihydroxy-octadecanoic acid; C16:0 diacid, hexadecanoic-1,16-dioic acid; and C18:2 diacid, linoleic-1,18-dioic acid.

there was no expression in other stages (Fig. 8, D, E, and H). No signal was detected in the negative control using sense *IPE1* transcript as a probe (Fig. 8I). This spatio-temporal specificity in *IPE1* expression is consistent with its role in modulating anther cuticle and pollen exine formation via the synthesis of aliphatic materials in the tapetum.

IPE1 Was Localized Mainly in the Endoplasmic Reticulum

There is a predicted secretory pathway signal peptide (SP) with 27 amino acids at the N terminus of the IPE1 protein according to the TargetP1.1 server (http://www.cbs.dtu.dk/services/TargetP/; Fig. 6Q). To investigate the cellular localization of the IPE1 protein, we generated three constructs: *pUbi*::*IPE1-GFP*, *pUbi*::*IPE1ΔSP-GFP*, and *pUbi*::*SP-GFP*. *pUbi*::*IPE1-GFP* contained the full-length IPE1 coding sequence fused to the 5′ terminus of GFP. In *pUbi*::*IPE1ΔSP-GFP*, the putative N-terminal signal peptide of the coding sequence was deleted and fused to GFP. *pUbi*::*SP-GFP* represented the DNA fragment of the putative N-terminal signal peptide fused with GFP. These constructs including *pUbi*::*GFP* were cointroduced with the endoplasmic

Table I. *Total fatty acids of wild-type and ipe1 anthers*

Fatty acid values shown are means ± SD.

Lipids	Wild Type	*ipe1*	Up
	$\mu g\ mg^{-1}$ *dry weight*		
C14:0 acid	0.066 ± 0.001	0.061 ± 0.009	−7.62%
C16:1 acid	0.041 ± 0.005	0.137 ± 0.029	234.37%
C16:0 acid	10.173 ± 1.060	4.285 ± 0.790	−57.88%
C17:0 acid	8.240 ± 0.043	8.268 ± 0.054	0.33%
C18:2 acid	15.055 ± 1.477	12.666 ± 2.573	−15.87%
C18:3 acid	26.167 ± 4.709	3.715 ± 0.487	−85.80%
C18:1 acid	0.257 ± 0.017	0.463 ± 0.104	80.59%
C18:0 acid	0.623 ± 0.066	0.890 ± 0.117	42.77%
C20:0 acid	0.457 ± 0.042	0.727 ± 0.067	59.27%
C22:0 acid	0.158 ± 0.008	0.398 ± 0.030	151.65%
C24:0 acid	0.099 ± 0.008	0.292 ± 0.039	195.92%
C26:0 acid	0.038 ± 0.003	0.092 ± 0.008	141.41%
C28:0 acid	0.140 ± 0.018	0.158 ± 0.048	12.83%
Total acids	61.513 ± 7.456	32.150 ± 4.355	−47.73%

reticulum marker red fluorescent protein (RFP)-KDEL (Liu et al., 2012) into the protoplast isolated from the maize seeding. Observations by confocal laser scanning microscopy showed that the free GFP signal was distributed widely in the cytoplasm (Fig. 9, A–D). IPE1-GFP fluorescence coincided with the fluorescence of the endoplasmic reticulum (Fig. 9, E–H). In contrast, IPE1ΔSP-GFP fluorescence did not clearly colocalize with the fluorescence of the endoplasmic reticulum (Fig. 9, I–L). Furthermore, the putative signal peptide of IPE1 could transfer GFP to the endoplasmic reticulum (Fig. 9, M–P). Therefore, the IPE1 protein was located in the ER.

Independent Roles of *IPE1*, *MS26*, and *MS45* in Anther Development

According to reports in the Maize Genetics and Genomics Database, two cloned genes, *MS26* and *MS45*, had been reported to participate in microspore development. To elucidate in detail the roles of *IPE1*, *MS26*, and *MS45* in regulating anther cuticle and pollen exine development, phenotypes of these mutants were analyzed. Available studies indicate that both anther cuticle and pollen exine development can be divided mainly into two steps: the formation of anther cuticle followed by maturation, and the formation of the three-layer structure of pollen exine followed by thickening (Li et al., 2010; Qin et al., 2013). Similar to the *ipe1* phenotype, the outer surface of *ms26* anthers was smooth at the mature pollen grain stage, and pollen exine did not form the typical three-layer structure at the late uninucleate microspore stage (Fig. 10, B and F). Compared with *ipe1* and *ms26*, the *ms45* anther epidermis was not glossy but lacked the normal reticular pattern (Fig. 10D). The typical three-layer structure of the pollen exine was well organized but thinner than that of the wild type (Fig. 10H). These results demonstrated that the similar functions of *IPE1* and *MS26* differed from that of *MS45*: *IPE1* and *MS26* are involved in the formation of the anther cuticle and pollen exine, whereas *MS45* serves in anther cuticle maturation and pollen exine thickening.

Expression analysis showed that *MS26* and *MS45* expression was observed only in young spikelets and was higher in anthers at the early uninucleate microspore stage (Supplemental Fig. S7). Subsequently, we investigated transcript levels of *MS26* and *MS45* in wild-type and *ipe1* anthers at the early uninucleate microspore stage, and no distinct difference was detected. Similarly, the expression of *IPE1* and *MS45* in *ms26* and the expression of *IPE1* and *MS26* in *ms45* did not differ (Fig. 10I). These results suggested that these three genes act independently in controlling anther development.

Transcriptome Analysis of Wild-Type and *ipe1* Anthers

To further dissect the regulatory network of *IPE1* during anther cuticle and pollen wall development, we performed transcript profiling of *ipe1* anthers at the early uninucleate microspore stage by RNA sequencing (RNA-Seq) technology. Using a cutoff (false discovery rate < 0.05 and fold change > 2), we identified 3,085 differentially expressed genes (DEGs), including 1,218 up-regulated genes and 1,867 down-regulated genes, in *ipe1* anthers. To validate the results, we randomly selected nine DEGs for qRT-PCR (Supplemental Fig. S8). The correlation of fold change values between RNA-Seq and qRT-PCR was 0.98, indicating that our RNA-Seq data were reliable. The analysis of Gene Ontology (GO) term enrichment indicated that the DEGs were involved in many biology processes, some of which were related to anther cuticle and microspore development, such as lipid biosynthetic processes and carbohydrate metabolic processes (Supplemental Fig. S9).

Fatty acid synthesis and elongation are essential for the formation of anther cuticle and pollen exine, which involve many enzymatic conversions. In plants, heteromeric acetyl-CoA carboxylase and fatty acid synthase are involved in de novo fatty acid biosynthesis, occurring in plastids and resulting in acyl-ACP moieties that are 16 or 18 carbons long (O'Hara et al., 2001). In *ipe1* anthers, the expression of two genes (*GRMZM2G124335* and *GRMZM2G072205*) involved in fatty acid biosynthesis was decreased (Table II). Very-long-chain fatty acids can be synthesized by a fatty acid elongase, 3-ketoacyl-CoA synthase, in vegetative tissues (Todd et al., 1999). Our results showed that transcription levels of 11 genes encoding β-ketoacyl-CoA synthase were altered in *ipe1* (Table II). Alkanes are the main component of wax. In Arabidopsis, the protein ECERIFERUM1 (CER1) is associated with long-chain alkane synthesis and pollen exine development (Aarts et al., 1995). In our study, *GRMZM2G066578*, a homolog of *CER1*, was down-regulated in *ipe1* anthers. However, another wax synthesis gene, *GRMZM2G114642*, was up-regulated (Table II).

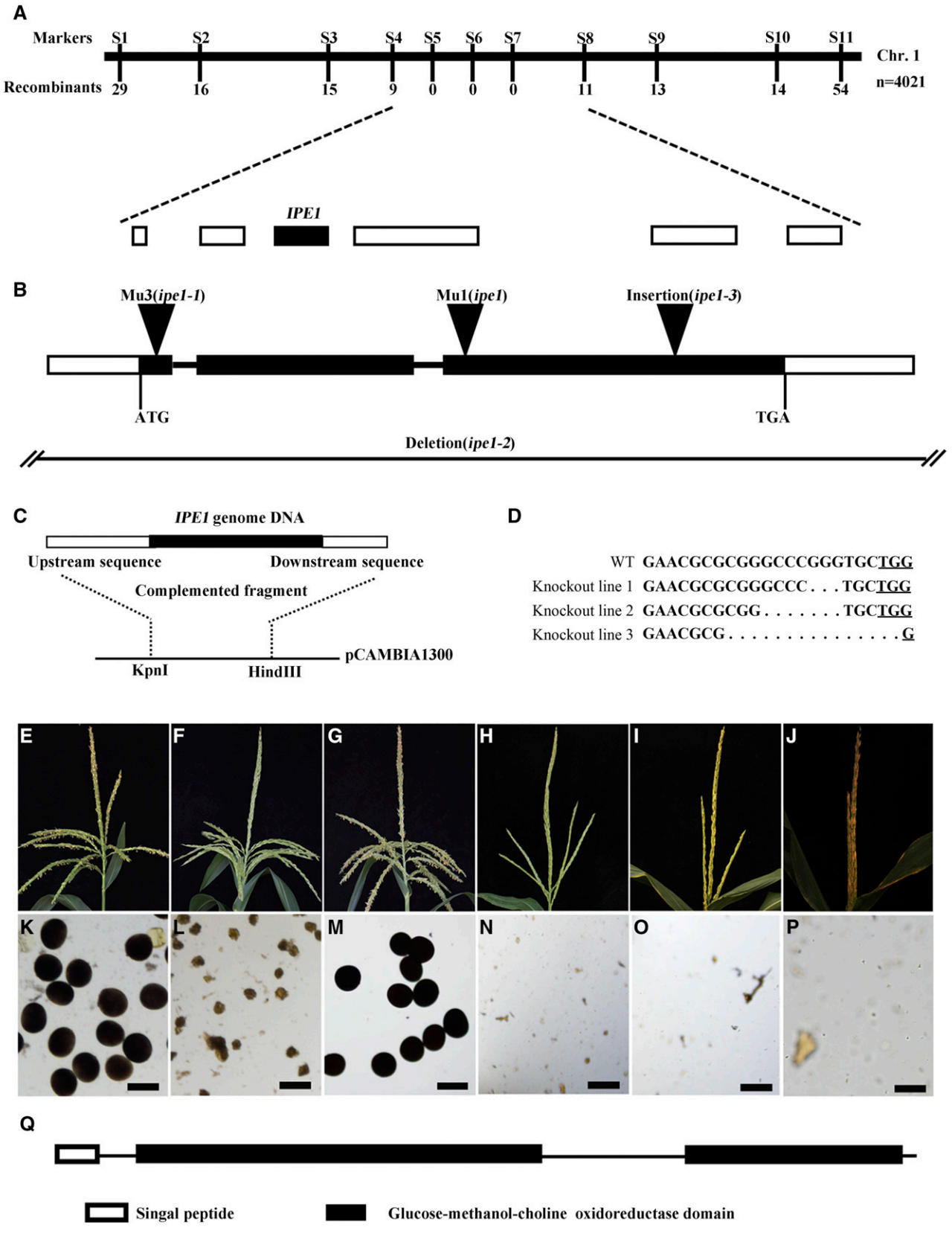

Figure 6. Positional cloning and confirmation of the *IPE1* gene. A, Fine-mapping of the *IPE1* gene. The *IPE1* locus was mapped to a 290-kb region between genetic markers S4 and S8 on the chromosome 1 short arm, containing six genes. Three Indel markers

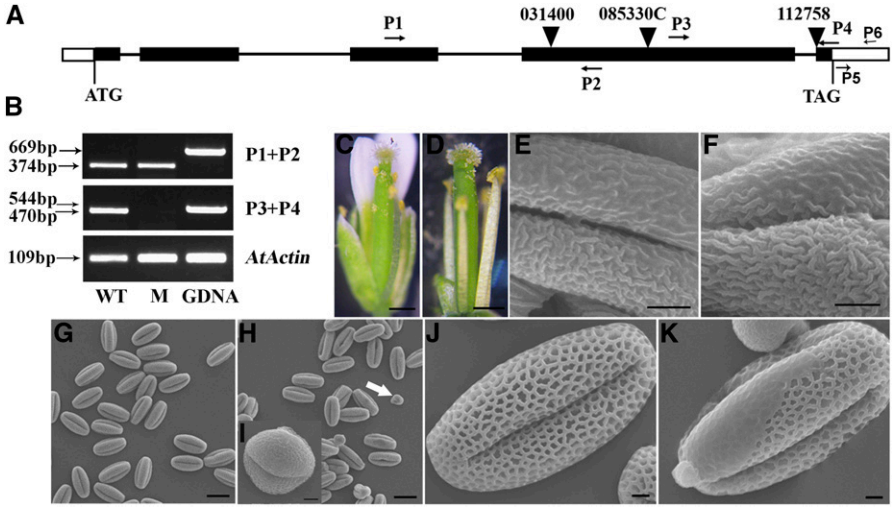

Figure 7. Phenotypic analysis of a T-DNA insertional line of the *IPE1* orthologous gene in Arabidopsis. A, Gene structure and the position of the T-DNA insertion in *AT1G12570*. B, Reverse transcription (RT)-PCR analysis with the primers shown in A. Amplification occurred with primers P1+P2 in the T-DNA insertional line but failed with primers P3+P4. *AtACTIN* was used as a positive control. WT, Wild type; M, T-DNA insertional line; GDNA, genomic DNA. C and D, The pollen grains of the wild type (C) and the T-DNA insertional line (D) are observed. E to K, SEM analysis of the wild type and the T-DNA insertional line. E and F, The normal anther surfaces of the wild type (E) and the T-DNA insertional line (F) are shown. G and H, Smaller pollen grains appeared in the T-DNA insertional line (arrow; H) compared with the wild type (G). I, Magnification of a smaller pollen grain. J and K, A few limited areas without a visible exine network were detected in the T-DNA insertional line (K) compared with the wild type (J). Bars = 500 μm in C and D, 2 μm in E, F, and I to K, and 20 μm in G and H.

Flavonoids also were considered constituents of the pollen wall, and several genes participating in flavonoid metabolism were identified. The expression of five genes involved in the synthesis of chalcones was altered, including two down-regulated genes (*GRMZM2G422750* and *GRMZM2G151227*) and three up-regulated genes (*GRMZM2G346095*, *GRMZM2G175812*, and *GRMZM2G114471*; Table II).

DISCUSSION

IPE1 Is Crucial for the Development of the Anther Cuticle and Pollen Exine in Maize

In this study, we showed that *ipe1* anthers exhibited a smooth outer surface of the epidermis (Fig. 3G; Supplemental Fig. S3). However, there were no apparent differences in the cuticular structures of stems, leaves, and glumes between the wild type and *ipe1* (Supplemental Fig. S10), which was consistent with the expression of the *IPE1* gene being detected only in the anther (Fig. 8A). The outer surface phenotype of *ipe1* anthers was very similar to that of mutants defective in the formation of the anther cuticle, such as *wda1* (Jung et al., 2006), *dpw* (Shi et al., 2011), *cyp704b2* (Li et al., 2010), *cyp703a3* (Yang et al., 2014), *osabcg15* (Niu et al., 2013; Qin et al., 2013), *osabcg26* (Zhao et al., 2015), and *tdr* (Li et al., 2006), in rice. Therefore, *IPE1* plays a vital role in the development of the anther cuticle in maize.

The anther cuticle is made of cuticular wax and cutin synthesized in the tapetum. In this study, we detected 17.37 ng mm^{-2} total wax and 601.79 ng mm^{-2} total

Figure 6. (*Continued.*)
(S5, S6, and S7) cosegregated with the male-sterile phenotype. B, Structure and mutation sites of the *IPE1* gene. Black boxes indicate exons, intervening lines indicate introns, and white boxes indicate untranslated regions. The triangles represent the locations of the insertions. In the *ipe1-2* mutant, there is a deletion containing the *IPE1* gene. C, The complemented fragment contains a 1,644-bp upstream sequence, the 2,585-bp *IPE1* genomic DNA, and a 969-bp downstream sequence after the stop codon. D, Mutation sites of three knockout lines generated by CRISPR-Cas9. Compared with the wild-type sequence (WT), the deletions of three nucleotides, seven nucleotides, and 15 nucleotides were detected in knockout lines 1, 2, and 3, respectively. Sequences in boldface, Target sites; dots, deleted nucleotides; underlined TGG, protospacer-adjacent motif sequences. E to P, Phenotypes of tassels (E–J) and pollen grains stained with 1% I_2-KI solution (K–P) at the mature pollen grain stage. E and K, Wild-type tassel and mature pollen grains. F and L, The *ipe1-3* anthers could not be exserted from glumes, and the pollen grains are abnormal. G and M, The complemented line of *ipe1-3* was restored to the wild-type phenotype. H to J and N to P, In knockout lines 1 (H and N), 2 (I and O), and 3 (J and P), the anthers could not be spread from glumes, and no pollen grains remain in the anther loculus. Bars = 100 μm. Q, The IPE1 protein contains a signal peptide at the N terminus and two Glc-methanol-choline oxidoreductase domains.

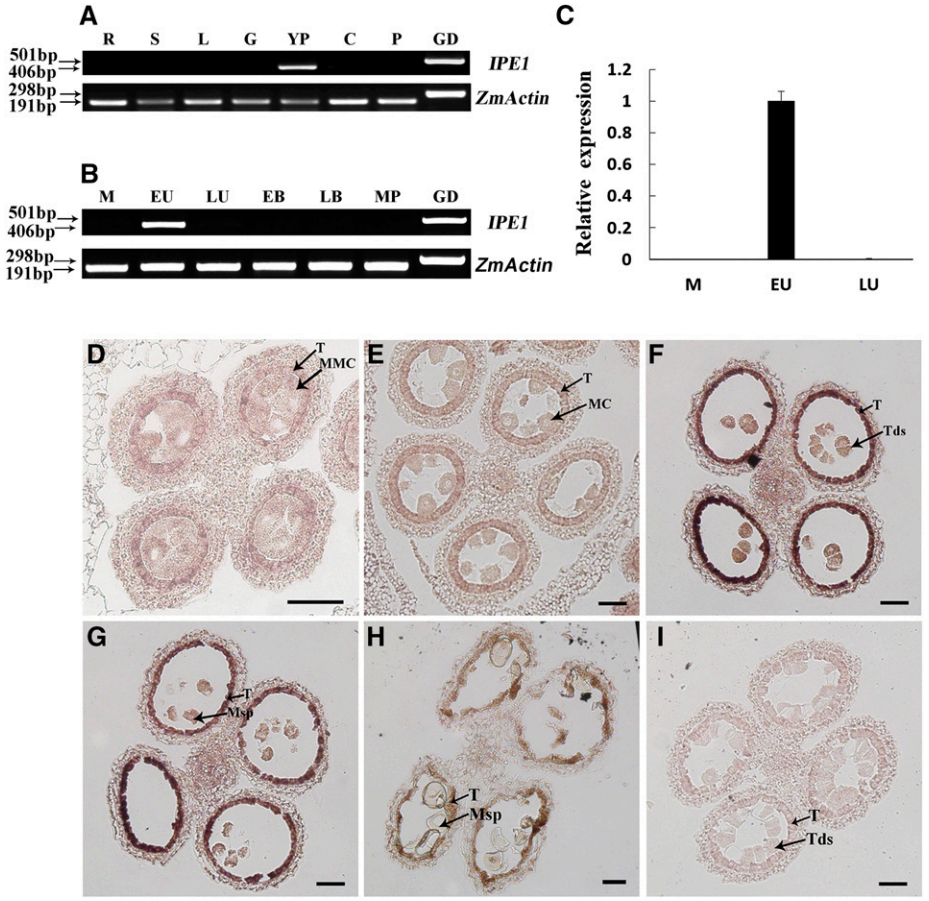

Figure 8. Expression analysis of the *IPE1* gene. A, Detection of *IPE1* transcript in wild-type selected tissues by RT-PCR, showing that *IPE1* was expressed only in the young spikelets. *ZmACTIN* was used as a positive control. R, Roots; S, stems; L, leaves; G, glumes; YP, young spikelets; C, cobs; P, pistils; GD, genomic DNA. B, Detection of *IPE1* transcript in wild-type anthers at different developmental stages by RT-PCR, showing that *IPE1* was restricted temporally to the anthers during the early uninucleate microspore stage. M, Meiosis stage; EU, early uninucleate microspore stage; LU, late uninucleate microspore stage; EB, early binucleate microspore stage; LB, late binucleate microspore stage; MP, mature pollen grain stage. C, qRT-PCR analysis of *IPE1* expression in wild-type anthers. Each data point is the average of three biological replicates. Error bars indicate SD ($n = 3$). D to I, RNA in situ hybridization of wild-type anthers using an *IPE1*-specific antisense probe (D–H) and a negative control sense probe (I). A strong hybridization signal in the tapetum was detected at the tetrad stage (F) and early uninucleate microspore stage (G). The signal in the tapetum disappeared at the early meiosis stage (D), meiosis stage (E), and late uninucleate microspore stage (H). Hybridization with the sense probe produced no signal at the tetrad stage (I). MC, Meiotic cell; MMC, meiotic mother cell; Msp, microspore; T, tapetum; Tds, tetrads. Bars = 50 μm.

cutin in wild-type anthers, suggesting that cutin is the major component of maize anther epidermis compared with the wax. Furthermore, the levels of total cutin and all cutin monomers in the *ipe1* mutant were decreased significantly while that of total wax was not obviously affected, indicating that the function of *IPE1* is involved in the synthesis of cutin. However, in the Arabidopsis *hothead-12* (*hth-12*) mutant, a homolog of *IPE1*, most of the cutin monomer remains unchanged, except for a reduction in the amount of C16 and C18 α-,ω-dicarboxylic acids and an increase in that of ω-hydroxy acids (Kurdyukov et al., 2006). This disagreement between the metabolic changes in maize and Arabidopsis may result from the fact that the functions of *IPE1* in maize and *HTH* in Arabidopsis are diverse. *IPE1* is involved in anther cuticle and pollen wall formation, and *HTH* is involved in the fusions of floral buds. Moreover, *IPE1* in maize may have less redundancy than in Arabidopsis. Surprisingly, a significant change of *ipe1* anther wax constituents was detected (Fig. 5). Therefore, we assumed that *IPE1* controls wax metabolism by feedback regulation. Consistent with this assumption, our RNA-Seq data showed that the expression of two wax synthesis genes was altered in the mutant (Table II). It should be noted that fatty acids are important precursors of anther wax and cutin (Shi et al., 2015). Chemical analysis revealed that *ipe1* anthers had a dramatic reduction in fatty acids (Table I), which was further confirmed by the fact that 11 genes involved in fatty acid synthesis and elongation were expressed differently in *ipe1* (Table II). Taken together, these data

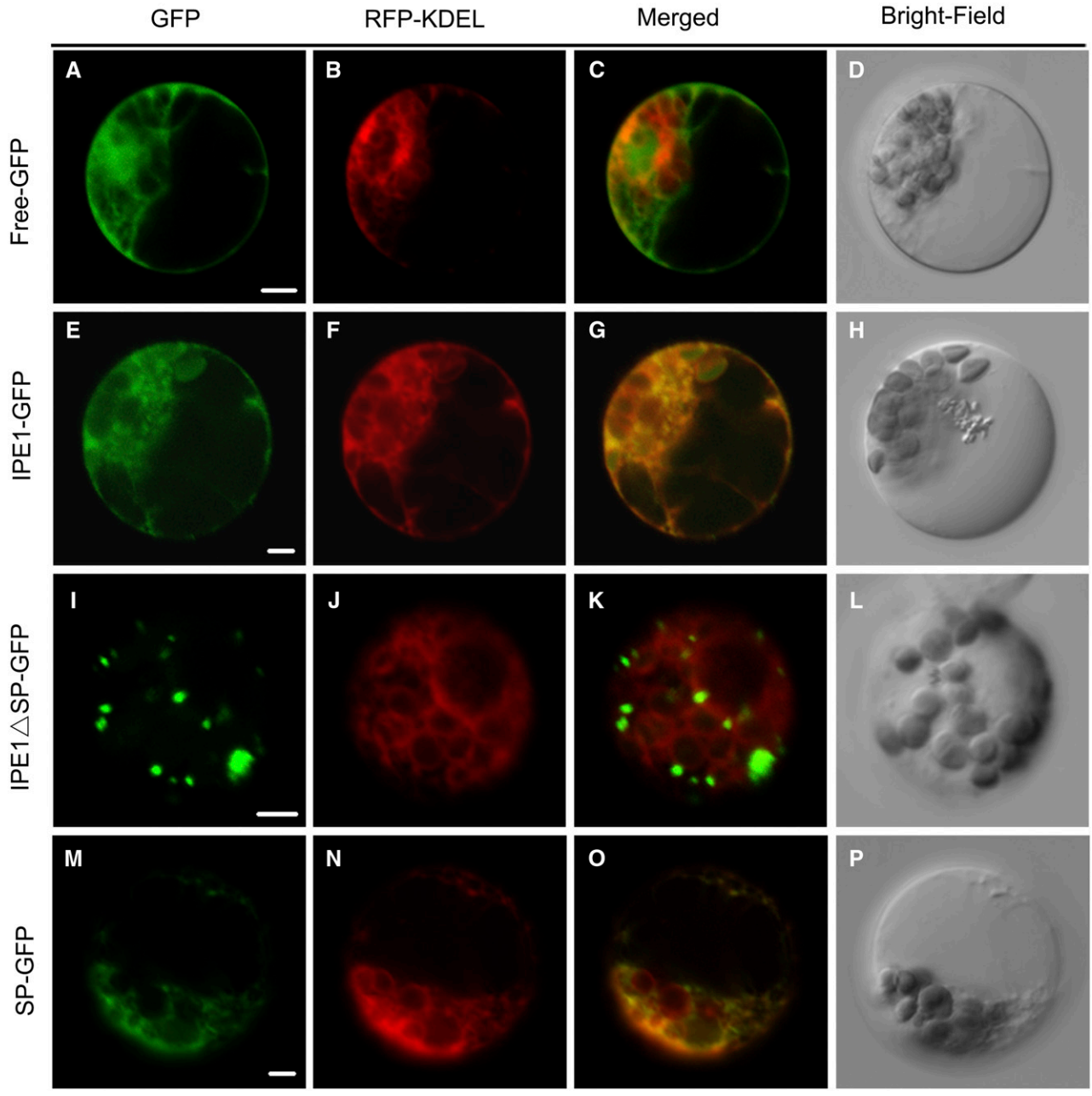

Figure 9. Subcellular localization of the IPE1 protein in maize protoplasts. A to D, A maize protoplast showing green fluorescent signals by expressing *pUbi*::*GFP* (A), red fluorescent signals by expressing the endoplasmic reticulum marker RFP-KDEL (B), merged signals (C) of A and B, and bright field (D). E to H, A maize protoplast showing green fluorescent signals by expressing *pUbi*::*IPE1-GFP* (E), red fluorescent signals by expressing the endoplasmic reticulum marker RFP-KDEL (F), merged signals (G) of E and F, and bright field (H). I to L, A maize protoplast showing green fluorescent signals by expressing *pUbi*::*IPE1ΔSP-GFP* (I), red fluorescent signals by expressing the endoplasmic reticulum marker RFP-KDEL (J), merged signals (K) of I and J, and bright field (L). M to P, A maize protoplast showing green fluorescent signals by expressing *pUbi*::*SP-GFP* (M), red fluorescent signals by expressing the endoplasmic reticulum marker RFP-KDEL (N), merged signals (O) of M and N, and bright field (P). Bars = 5 μm.

suggested that the *IPE1* mutation leads to the alteration of anther aliphatic molecules, eventually resulting in abnormal anther cuticle.

The tapetum is essential for sporopollenin deposition and pollen exine synthesis, which commence at the tetrad stage; the structure of the pollen exine is evident at the uninucleate microspore stage. Afterward, the size increases gradually (Blackmore et al., 2007). Our TEM observations revealed that sporopollenin deposition and the morphology of *ipe1* pollen exine were defective, due to the bacula being undeveloped at the early uninucleate microspore stage (Fig. 4, N and X). Similarly,

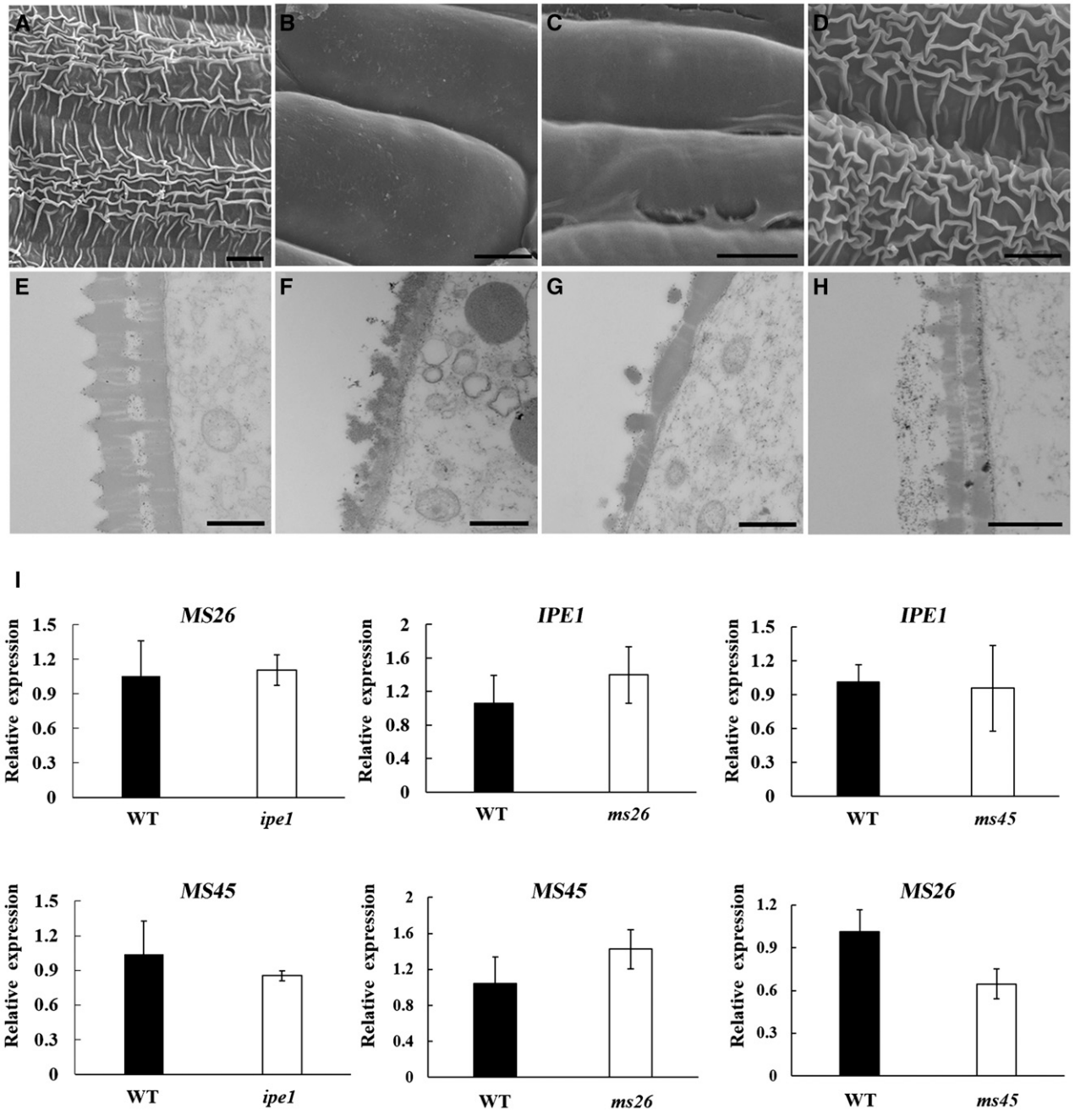

Figure 10. Phenotypic and expression analyses of *IPE1*, *MS26*, and *MS45*. A to D, Scanning electron micrographs of the anther outer surface at the mature pollen grain stage. The mature reticular anther cuticle was observed in the wild type (A), while its formation was disturbed in *ms26* (B) and *ipe1* (C), and *ms45* anther cuticle did not mature normally (D). Bars = 6 μm. E to H, Transmission electron micrographs of the pollen wall at the late uninucleate microspore stage. The wild-type pollen exine had three thick layers composed of the tectum, bacula, and nexine (E), whereas the pollen exine of *ms26* (F) and *ipe1* (G) did not form the three-layer structure, and the thickening of pollen exine was affected in the *ms45* mutant (H). Bars = 0.5 μm. I, Transcript levels of *IPE1*, *MS26*, and *MS45* in reciprocal mutants, showing that their expression was not apparently altered by reciprocal mutations. WT, Wild type. Values are means ± SD of three replicates.

the development of bacula structure and pollen exine is disrupted in rice *tdr* (Zhang et al., 2008) and *cyp704b2* (Li et al., 2010) and Arabidopsis *acyl-coa synthetase5* (de Azevedo Souza et al., 2009). These data indicated that the bacula is indispensable for the sporopollenin deposition required for pollen exine synthesis. In addition, the abnormal pollen exine resulted from the dysfunction of Ubisch bodies in transferring sporopollenin precursors

Table II. *A selection of DEGs putatively involved in anther cuticle and pollen exine development*

Gene Identifier	Gene Description	Log_2 (*ipe1*/Wild Type)
GRMZM2G066578	Wax synthesis	−4.28
GRMZM2G114642	Wax synthesis	4.67
GRMZM2G422750	Chalcone synthase	−3.56
GRMZM2G151227	Chalcone synthase	−6.66
GRMZM2G346095	Chalcone synthase	2.38
GRMZM2G175812	Chalcone synthase	4.93
GRMZM2G114471	Chalcone synthase	2.69
GRMZM2G124335	Ketoacyl-ACP synthase	−3.55
GRMZM2G072205	Ketoacyl-ACP synthase	−4.67
GRMZM2G022558	β-Ketoacyl-CoA synthase	−2.58
GRMZM2G162508	β-Ketoacyl-CoA synthase	−2.67
GRMZM2G168304	β-Ketoacyl-CoA synthase	−2.14
GRMZM2G445602	β-Ketoacyl-CoA synthase	−3.34
GRMZM2G164974	β-Ketoacyl-CoA synthase	−1.73
GRMZM2G003501	β-Ketoacyl-CoA synthase	−2.42
GRMZM2G063024	β-Ketoacyl-CoA synthase	−3.59
GRMZM2G097469	β-Ketoacyl-CoA synthase	3.19
GRMZM2G149636	β-Ketoacyl-CoA synthase	2.07
GRMZM2G075140	β-Ketoacyl-CoA synthase	2.41
GRMZM2G003138	β-Ketoacyl-CoA synthase	3.22

(Fig. 4T). Furthermore, *IPE1* was expressed specifically in anthers during the tetrad and uninucleate microspore stages (Fig. 8, F and G), when the primexine and bacula were developing. Strikingly, *IPE1* was expressed mainly in the tapetum, where sporopollenin precursors were synthesized. Collectively, our data indicated that IPE1 is crucial for pollen exine development.

IPE1 Mediates the Lipid Metabolic Pathway in the Tapetum

Hydroxyacids and dicarboxylic acids are the important constituents of the protective cuticle in anthers (Li et al., 2010; Shi et al., 2011). However, the mechanism underlying the conversion from hydroxyacids to dicarboxylic acids in the reproductive organs is little known. It is believed that modifications of fatty acids from the plastid occur in the endoplasmic reticulum, which contributes to anther cuticle and pollen wall development (Kunst and Samuels, 2003; Lallemand et al., 2013). In our work, we cloned a novel maize male-sterile gene, *IPE1*, putatively encoding a member of the GMC oxidoreductase superfamily. Further analysis revealed that the IPE1 protein was targeted to the endoplasmic reticulum (Fig. 9). These results supported the hypothesis that IPE1 regulates fatty acid metabolism.

GMC oxidoreductases have a wide variety of substrates and can catalyze the oxidation of an alcohol to the corresponding aldehyde (Dreveny et al., 2001; Wongnate and Chaiyen, 2013). In Arabidopsis, the ADHESION OF CALYX EDGES (ACE)/HTH protein was found to be a single-domain protein related to GMC oxidoreductase domain-containing proteins and could oxidize long-chain ω-hydroxy fatty acids produced in the ω-oxidation pathway of cytochrome P450 fatty acid ω-hydroxylases. Supportively, the content of α-,ω-dicarboxylic fatty acids has been found to decrease and that of ω-hydroxy fatty acids to increase in the *ace/hth* mutant, resulting in defects in cuticle development (Krolikowski et al., 2003; Kurdyukov et al., 2006). Meanwhile, the biochemical activity of ω-hydroxyacid dehydrogenase and ω-oxoacid dehydrogenase has been proven in epidermis of young *Vicia faba* leaves and potato (*Solanum tuberosum*) discs (Kolattukudy et al., 1975; Agrawal and Kolattukudy, 1977). Consistently, an abnormal anther cuticle and the significant reduction of C16:0 and C18:2 diacids were observed in the *ipe1* mutant. However, in contrast to the *ace/hth* mutant, the amount of ω-hydroxy fatty acids detected in *ipe1* anthers and C16 and C18 fatty acids was reduced dramatically. The discrepancy could be explained by the following reasons. (1) In lipid metabolism, some other genes are involved in the metabolism of C16 and C18 fatty acids and C16/C18 ω-hydroxy fatty acids, such as *POLYKETIDE SYNTHASE A* and *POLYKETIDE SYNTHASE B* (Kim et al., 2010). *IPE1* may regulate their metabolism by the feedback pathway. (2) Mutation of the *IPE1* gene leads to wilted anthers, which may cause

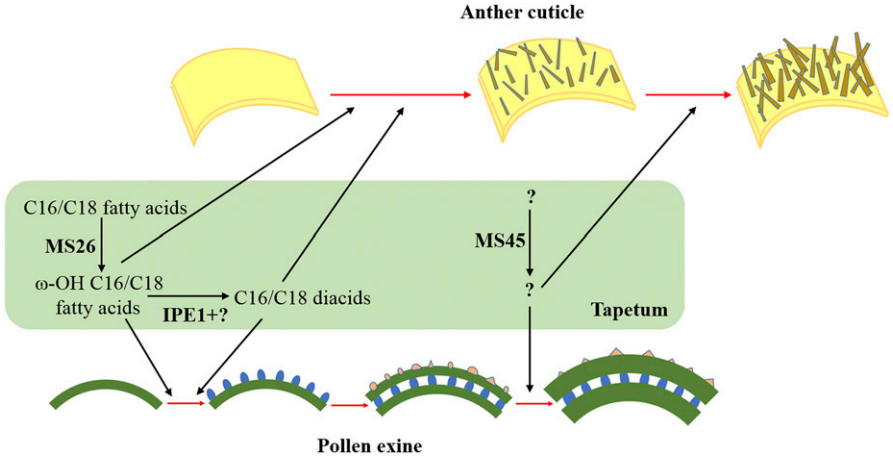

Figure 11. Model for the role of IPE1 during anther cuticle and pollen exine development. C16/C18 fatty acids synthesized in the plastid are transported to the endoplasmic reticulum and hydroxylated to ω-hydroxy C16/C18 fatty acids by MS26. After IPE1 and an aldehyde dehydrogenase reaction, ω-hydroxy C16/C18 fatty acids are converted to C16/C18 diacids. ω-Hydroxy C16/C18 fatty acids and C16/C18 diacids are required for anther cuticle and pollen exine formation. The product formed by MS45 is involved in the maturation of the anther cuticle and thickening of the pollen exine.

the degradation of some fatty acids. In addition, MS26 may hydroxylate C16 and C18 fatty acids at the ω-carbon position (Dobritsa et al., 2009; Li et al., 2010; Djukanovic et al., 2013). To sum up, we speculate that the major function of *IPE1* in anther development is as follows: ω-hydroxy C16/C18 fatty acids formed by MS26 can be converted into C16/C18 diacids by IPE1 in the tapetum and long-chain ω-aldehyde dehydrogenases, which will further enrich the lipid metabolic pathway in anthers, especially the formation of dicarboxylic acids. Surprisingly, C16/C18 diacids only account for less than 1% of the total amount of cutin in our study. How do the diacids play the vital role in anther development? This may be caused by the following reasons. (1) The diacids are not the main constituent but are a crucial constituent for anther cuticle and pollen exine development. (2) The altered conversion from hydroxy C16/C18 fatty acids to C16/C18 diacids will result in the disruption of other metabolic pathways involved in cutin and wax synthesis. Compared with previous reports (Li et al., 2010; Shi et al., 2011), we detected that the C18:0 9/10 di-OH diacid is a cutin monomer and that the level is reduced significantly in the mutant, indicating that *IPE1* participates in the metabolism of the C18:0 9/10 di-OH diacid indirectly.

Interestingly, our phenotypic analysis found that the tapetum was degraded early in the mutant (Figs. 2R and 4R), consistent with the preferential expression patterns of *IPE1* in tapetum, suggesting that *IPE1* can control tapetal development. Transcription factors are the master regulator of the development of tapetal cells and pollen exine. In Arabidopsis and rice, many genes encoding enzymes needed for wax, cutin, and sporopollenin biosynthesis can be modulated by transcription factors (Shi et al., 2015). For example, *CYP703A3*, encoding a cytochrome P450 fatty acid hydroxylase, can be regulated by GAMYB and TDR and can be involved in tapetal degradation (Yang et al., 2014). In Arabidopsis, *DYSFUNCTIONAL TAPETUM1* (Gu et al., 2014), *ABORTED MICROSPORES* (Xu et al., 2010, 2014), and *MS1* (Wilson et al., 2001; Ito et al., 2007; Yang et al., 2007) can regulate multiple genes involved in pollen wall development. Thus, we hypothesized that IPE1 indirectly regulates tapetal degeneration via transcription factors.

IPE1, MS26, and MS45 Cooperatively Regulate Anther Cuticle and Pollen Exine Development in an Independent Manner

Aliphatic materials containing wax, cutin, and sporopollenin share one common catalytic pathway in the tapetum, and they will be transported to the surface of anthers and microspores (Zhao et al., 2015). In maize, knowledge about the development of the anther cuticle and pollen exine is limited (Cigan et al., 2001; Skibbe and Schnable, 2005; Djukanovic et al., 2013). In this study, we compared three male-sterile mutants of maize (*ipe1*, *ms26*, and *ms45*) in which the phenotypes of pollen exine and anther cuticle were all defective (Fig. 10, A–H). In accordance with that, the three genes were expressed specifically in the anthers (Fig. 8A; Supplemental Fig. S7). Furthermore, *IPE1* and *MS45* were expressed mainly in the tapetum (Cigan et al., 2001; Fig. 8, D–I). In addition, *CYP704B2*, the rice homolog of *MS26*, also was expressed in the tapetum (Li et al., 2010). The phenotypes of *ipe1*, *ms26*, and *ms45*, coupled with their expression patterns, suggested that *IPE1*, *MS26*, and *MS45* are all required for anther cuticle and pollen exine development. However, their phenotypes were different: the anther outer surface was smooth in *ipe1* and *ms26*, while in *ms45*, it was not smooth but lacked the regular reticular structure, implying that *IPE1* and *MS26* play a role in the formation of the anther cuticle whereas *MS45* functions in its maturation. The three layers of pollen exine did not form in *ipe1* and *ms26* and appeared but did not thicken in *ms45*, indicating that *IPE1* and *MS26* initiate pollen exine formation and *MS45* enhances its thickness. Furthermore, expression pattern analysis of the three genes suggested that they function independently in anther development (Fig. 10I).

Taken together, we propose an initial working model of how IPE1 regulates anther cuticle and pollen wall development in maize (Fig. 11). In the tapetum, MS26 functions as a cytochrome P450 monooxygenase to generate ω-hydroxy C16/C18 fatty acids, which can be oxidized to C16/C18 dioic acids by IPE1 and corresponding aldehyde dehydrogenases. ω-Hydroxy C16/C18 fatty acids and dioic acids can be transferred to the surface of anthers and microspores to form the anther cuticle and the three layers of pollen exine. Afterward, the MS45 product participates in the maturation of the anther cuticle and thickening of the pollen exine.

MATERIALS AND METHODS

Plant Materials and Growth Conditions

Maize (*Zea mays*) *mu1019442*::*Mu* (*ipe1-1*), *ms*-6044*(*ipe1-3*), *ms26*, and *ms45-6006* (*ms45*) were obtained from the Maize Genetics Cooperation Stock Center. *ipe1-2* was a radiation-treated mutant. The Arabidopsis (*Arabidopsis thaliana*) T-DNA insertional lines were from The Arabidopsis Information Resource. All maize materials with the exception of *ms*-6044*(*ipe1-3*) were grown in experimental stations of the China Agricultural University in Beijing and San Ya. *ms*-6044*(*ipe1-3*) was grown in experimental stations of the Institute of Genetics and Developmental Biology of the Chinese Academy of Sciences in Beijing and San Ya. The maize transgenic plants and population were grown in a greenhouse of the Institute of Genetics and Developmental Biology. *ipe1* was backcrossed to inbred line zheng58 five times for morphological comparisons. Arabidopsis lines were grown in a greenhouse under 16 h of light/8 h of dark at 22°C.

Characterization of Phenotypes

A Nikon D40 digital camera or Olympus SZX10 dissecting microscope was used to take photographs for plants and flowers.

For SEM, anthers at different stages were prefixed in 2.5% glutaraldehyde overnight at 4°C and then rinsed three times using phosphate-buffered saline (pH 7.2). Samples were postfixed for 1 h in 1% osmium tetraoxide and rinsed three times using phosphate-buffered saline. The samples were dehydrated using a graded ethanol series (30%–100%) and then rinsed three times with isoamyl acetate. The samples were critical point dried and gold coated. The observation and recording of images were performed using a Hitachi S-3400N scanning electron microscope.

For TEM analysis, anthers were vacuum infiltrated and prefixed in 2.5% glutaraldehyde followed by rinsing with 0.1 M phosphate buffer. The samples were fixed in 1% osmium tetraoxide and rinsed with 0.1 M phosphate buffer. The fixed samples were dehydrated using an acetone series from 30% to 100% and embedded in epoxy resin. Ultra-thin sections were prepared using a Leica UC6 I ultramicrotome and were stained with uranyl acetate and double stained with lead citrate. Images were obtained with a JEM-1230 transmission electron microscope.

For meiosis analysis, young panicles from the wild type and *ipe1* were harvested and fixed in Carnoy's solution (ethanol:glacial acetic acid, 3:1, v/v). Anthers undergoing meiosis were crushed with forceps in an acetocarmine solution on glass slides and then covered with a cover slip. First, slides were examined with a light microscope, and then cover slips of ideal slides were removed in liquid nitrogen. Chromosomes were stained with DAPI, and images were captured with an Olympus BX61 fluorescence microscope.

Analysis of Anther Wax, Cutin, and Fatty Acids

To describe amounts per unit of surface area, we determined a ratio of anther weight to surface area (Supplemental Fig. S2). The area was calculated according to the length and width of anthers in microscope images, assuming a cylindrical body for maize anthers. To extract waxes, 200 mg of fresh anther sample corresponding to 1,521 to 2,292 mm^2 of surface area was submersed in 3 mL of chloroform for 1 min. The resulting chloroform extracts were spiked with 30 μg of docosanol and 10 μg of heptadecanoic acid as internal standards and transferred to a new vial. The solvents were evaporated under a gentle stream of nitrogen gas. The residue was derivatized with 100 μL of *N*-methyl-*N*-(trimethylsilyl) trifluoroacetamide and incubated for 1 h at 50°C. To extract anther cutin, the remaining anthers were submersed in 3 mL of chloroform: methanol (1:1, v/v). They were first incubated at 50°C for 30 min and then 72 h with constant shaking at room temperature. The anthers were freeze dried and submersed in 1 mL of 1 N methanolic HCl for 2 h at 80°C with 10 μg of heptadecanoic acid as an internal standard. The hydrophobic monomers were subsequently extracted three times with 1 mL of hexane after the addition of 2 mL of saturated NaCl solution. The solvent evaporated, and the remaining samples were derivatized as described above. These derivatized samples were then analyzed by GC-MS (Agilent gas chromatograph coupled to an Agilent 5975C quadrupole mass selective detector). The results of anther wax and cutin analysis were related to unit surface area.

To extract total fatty acids, 6 mg of freeze-dried anther material was transesterified in 1 mL of 1 N methanolic HCl (containing 50 μg of heptadecanoic acid as an internal standard) for 4 h at 50°C. After the addition of 1.5 mL of 0.9% (w/v) NaCl, the hydrophobic monomers were subsequently extracted with 1.5 mL of hexane. The organic phases were evaporated under a gentle stream of nitrogen gas. The residue was dissolved in 100 μL of hexane and then analyzed by GC-MS (Agilent gas chromatograph coupled to an Agilent 5975C quadrupole mass selective detector). The results of the total fatty acid analysis were related to unit dry weights of anthers.

Molecular Cloning and Allelism Test

ipe1 was crossed with inbred line zheng58, and the F1 plants were self-pollinated to generate an F2 population; individuals with mutations were chosen for the mapping population. Simple sequence repeat markers distributed on 10 chromosomes were used for initial mapping. For fine-mapping, several Indel markers were designed with Oligo7 software. Primers used for fine-mapping are listed in Supplemental Table S2. The genotype was confirmed with 3% agarose gels. For the allelism test, six genetic crosses were produced among *ipe1*, *ipe1-1*, *ipe1-2*, and *ipe1-3*, whose progeny were analyzed for the segregating ratio between fertility and sterility.

Complementation of the Mutant

For functional complementation of the maize *ipe1-3* mutant, the DNA fragment was obtained with primers 1F (5′-GAAGAAAGGTTGCGTCAG-3′) and 1R (5′-ATTGCGATGGGAGCGTAT-3′) and digested with *Hin*dIII and *Kpn*I. The digested fragment was cloned into the binary vector pCAMBIA1300 to generate the *p1300:IPE1* plasmids. These plasmids contained a 5,198-bp genomic fragment with the entire 2,585-bp *IPE1* gene region, a 1,644-bp upstream sequence region, and a 969-bp downstream region and were transformed into the maize hybrid Hi-II with *Agrobacterium tumefaciens* AGL1. We backcrossed the positive transgenic individuals to *ipe1-3* continuously twice to obtain positive transgenic plants with the *ipe1-3* background and assayed its mature pollen grains with 1% I_2-KI staining solution.

Constructs for CRISPR-Cas9 and Transformation

The vector pBUN411 from Genovo Biotech was used, and a 23-bp fragment from the second exon of *IPE1* (sequence as shown in Fig. 6D) was introduced into the vector and then used for *A. tumefaciens*-mediated transformation into maize (Hi-II). Transgenic plants were identified by the enzyme digestion reaction with *Xma*I/*Sma*I and PCR amplification using the primers 2F (5′-CGCCCCTGGTGTCGCAGTACA-3′) and 2R (5′-CGCCGACAGGATCACC-TCGTTC-3′). Mature pollen grains of transgenic lines were observed by I_2-KI staining.

Phylogenetic Analysis

The full-length amino acid sequence of IPE1 and 17 of the most similar sequences identified via a BLAST search were aligned with the ClustalW tool using default parameters. A phylogenetic tree was constructed with the alignment of IPE1-like protein sequence using MEGA 5 with the following parameters: Poisson model, complete deletion, and 1,000 bootstrap replicates.

RNA Extraction, RT-PCR, and qRT-PCR

Total RNA was isolated with TRIzol reagent (Invitrogen) from maize roots, stems, glumes, young spikelets, cobs, pistils, and anthers and Arabidopsis flowers. Total RNA (1.5 μg) was treated with *DNase* I (Promega), and RT was conducted using Moloney murine leukemia virus reverse transcriptase (Invitrogen) and oligo$(dT)_{20}$ primers. RT product (1 μL) was used as the template for PCR. qRT-PCR was performed on an ABI 7500 real-time PCR system with SYBR Green PCR Master Mix (Takara). *ZmACTIN* and *AtACTIN* were used as the internal normalization controls. Every sample contained three biological replications and three technological replications. Relative expression was calculated using the $2^{-\Delta\Delta Ct}$ method. The SD was calculated with three biological replications. All primers used for RT-PCR and qRT-PCR are listed in Supplemental Table S2.

In Situ Hybridization

The anthers of inbred line zheng58 at the different developmental stages were fixed overnight in 3.7% formalin-acetic acid-alcohol (3.7% formaldehyde, 5% glacial acetic acid, and 50% ethanol), dehydrated in a graded ethanol series (50%, 70%, 85%, 95%, and 100%), and then embedded in paraffin and sliced into 8-μm sections. The construct of the *IPE1* probe was generated with the gene-specific primer (primer sequence is given in Supplemental Table S2). Probe synthesis and RNA in situ hybridization were performed according to previously described protocols (Ding et al., 2015).

Subcellular Localization of IPE1

For the analysis of subcellular localization, three fragments (the 1,746-bp coding sequence without the stop codon [IPE1], the 1,653-bp coding sequence without the 93-bp fragment encoding the putative signal peptide and stop codon [IPE1ΔSP], and the N-terminal signal peptide-encoding sequence [SP]) were amplified with the primers GFP-F/R, ΔSP-GFP-F/GFP-R, and GFP-F/SP-GFP-R and cloned into pJIT163-GFP to obtain C-terminal fusions with GFP. Maize protoplasts were isolated as described (Yoo et al., 2007), and the endoplasmic reticulum marker RFP-KDEL (Liu et al., 2012) was cotransformed with the plasmids *pUbi::IPE1-GFP*, *pUbi::IPE1ΔSP-GFP*, *pUbi::SP-GFP*, and *pUbi::GFP* individually using the polyethylene glycol-mediated method. Transformed protoplasts were incubated on six-well plates in the dark at 23°C overnight. Fluorescence was determined with a fluorescence confocal microscope (Zeiss LSM 710).

RNA-Seq Analysis

Anthers were collected from the wild type and *ipe1* at the early uninucleate microspore stage, with two biological replicates for each genotype. Total RNA was extracted with TRIzol reagent (Invitrogen). Library construction was conducted according to Illumina TruSeq mRNA construction and sequenced on a HiSeq 2500 sequencer. Raw reads were preprocessed to remove low-quality

bases and cut adapter sequences by employing the SolexQA (Cox et al., 2010) and Cutadapt (Martin. 2011) tools. Clean reads were then mapped to the maize genome sequence (AGPv3; MaizeSequence.org) using TopHat (Trapnell et al., 2009) with default parameters. Read counts of annotated genes were obtained separately by HTSeq-count (Anders et al., 2015). Lowly expressed genes were removed, and only genes with an expression level of at least 1 count per million in at least two samples were retained for further analysis. The R package edgeR was then employed to identify the DEGs (Robinson et al., 2010). Genes with more than 2-fold change in expression level and a false discovery rate less than 0.05 were considered DEGs. GO terms for each maize gene were obtained at http://www.gramene.org/. The GO enrichment analysis for DEGs was done with the R package TopGO (Alexa et al., 2006). Adrian Alexi's improved weighted scoring algorithm and Fisher's exact test were used to determine the significance of GO term enrichment. A GO term with $P < 0.01$ was thought to be a significant enrichment GO term.

Accession Numbers

Sequence data from this article can be found in the GenBank/EMBL databases under the following accession numbers: *MS26*, NM_001137176.1; *MS45*, XM_008662089.1.

Supplemental Data

The following supplemental materials are available.

Supplemental Figure S1. DAPI staining of chromosomes of the wild type and *ipe1* in meiosis.

Supplemental Figure S2. Weight-surface area ratio of wild-type and *ipe1* anthers.

Supplemental Figure S3. SEM observation of the anther surface.

Supplemental Figure S4. Phylogenetic tree of IPE1-related proteins.

Supplemental Figure S5. Sequence alignment of IPE1 and 17 IPE1-related proteins.

Supplemental Figure S6. Phenotypes of two additional T-DNA insertional lines of *AT1G12570*.

Supplemental Figure S7. Spatial and temporal expression of *MS26* and *MS45* by RT-PCR.

Supplemental Figure S8. qRT-PCR analysis of nine randomly selected DEGs in *ipe1*.

Supplemental Figure S9. Significantly enriched GO terms of the up-regulated genes and down-regulated genes between the wild type and *ipe1*.

Supplemental Figure S10. SEM analysis of the surfaces of glume, leaf, and stem in the wild type and *ipe1*.

Supplemental Table S1. Detailed cutin compositions of wild-type and *ipe1* anthers.

Supplemental Table S2. Primers used in this study.

Supplemental Table S3. Fertile and sterile plant analysis of F1 plants from genetic crosses among *ipe1*, *ipe1-1*, *ipe1-2*, and *ipe1-3*.

Supplemental Table S4. Putative expression patterns of *IPEI* homologous genes.

ACKNOWLEDGMENTS

We thank Dr. Xiaolan Zhang (China Agricultural University) and Chunju An (China Agricultural University) for valuable comments in the preparation of this article; Caixia Gao (Institute of Genetics and Developmental Biology, Chinese Academy of Sciences) for providing the *pUbi*::*GFP* construct and for maize transformation; Fengxia Zhang (Institute of Genetics and Developmental Biology, Chinese Academy of Sciences) for wax, cutin, and fatty acid assays and primary analysis; and Yanbao Tian (Institute of Genetics and Developmental Biology, Chinese Academy of Sciences) for the subcellular localization of IPE1.

Received April 18, 2016; accepted November 11, 2016; published November 15, 2016.

LITERATURE CITED

Aarts MG, Keijzer CJ, Stiekema WJ, Pereira A (1995) Molecular characterization of the *CER1* gene of *Arabidopsis* involved in epicuticular wax biosynthesis and pollen fertility. Plant Cell **7:** 2115–2127

Agrawal VP, Kolattukudy PE (1977) Biochemistry of suberization: ω-hydroxyacid oxidation in enzyme preparations from suberizing potato tuber disks. Plant Physiol **59:** 667–672

Albertsen MC, Fox TW, Huffmann G, Trimnell M August 29, 2006. Nucleotide sequences affecting plant male fertility and methods of using same. United States Patent Application No. 7098388B2

Albertsen MC, Fox TW, Trinmell MR (1993) Cloning and utilizing a maize nuclear male sterility gene. Proc Annu Corn Sorghum Ind Res Conf **48:** 224–233

Alexa A, Rahnenführer J, Lengauer T (2006) Improved scoring of functional groups from gene expression data by decorrelating GO graph structure. Bioinformatics **22:** 1600–1607

Anders S, Pyl PT, Huber W (2015) HTSeq: a Python framework to work with high-throughput sequencing data. Bioinformatics **31:** 166–169

Ariizumi T, Toriyama K (2011) Genetic regulation of sporopollenin synthesis and pollen exine development. Annu Rev Plant Biol **62:** 437–460

Beisson F, Li-Beisson Y, Pollard M (2012) Solving the puzzles of cutin and suberin polymer biosynthesis. Curr Opin Plant Biol **15:** 329–337

Blackmore S, Wortley AH, Skvarla JJ, Rowley JR (2007) Pollen wall development in flowering plants. New Phytol **174:** 483–498

Chaubal R, Anderson JR, Trimnell MR, Fox TW, Albertsen MC, Bedinger P (2003) The transformation of anthers in the *msca1* mutant of maize. Planta **216:** 778–788

Cigan AM, Unger E, Xu R, Kendall T, Fox TW (2001) Phenotypic complementation of *ms45* maize requires tapetal expression of MS45. Sex Plant Reprod **14:** 135–142

Cox MP, Peterson DA, Biggs PJ (2010) SolexaQA: at-a-glance quality assessment of Illumina second-generation sequencing data. BMC Bioinformatics **11:** 485

de Azevedo Souza C, Kim SS, Koch S, Kienow L, Schneider K, McKim SM, Haughn GW, Kombrink E, Douglas CJ (2009) A novel fatty acyl-CoA synthetase is required for pollen development and sporopollenin biosynthesis in *Arabidopsis*. Plant Cell **21:** 507–525

Ding L, Yan S, Jiang L, Zhao W, Ning K, Zhao J, Liu X, Zhang J, Wang Q, Zhang X (2015) HANABA TARANU (HAN) bridges meristem and organ primordia boundaries through PINHEAD, JAGGED, BLADE-ON-PETIOLE2 and CYTOKININ OXIDASE 3 during flower development in *Arabidopsis*. PLoS Genet **11:** e1005479

Djukanovic V, Smith J, Lowe K, Yang M, Gao H, Jones S, Nicholson MG, West A, Lape J, Bidney D, et al (2013) Male-sterile maize plants produced by targeted mutagenesis of the cytochrome P450-like gene (*MS26*) using a re-designed I-CreI homing endonuclease. Plant J **76:** 888–899

Dobritsa AA, Shrestha J, Morant M, Pinot F, Matsuno M, Swanson R, Møller BL, Preuss D (2009) CYP704B1 is a long-chain fatty acid ω-hydroxylase essential for sporopollenin synthesis in pollen of Arabidopsis. Plant Physiol **151:** 574–589

Dong Z, Jiang C, Chen X, Zhang T, Ding L, Song W, Luo H, Lai J, Chen H, Liu R, et al (2013) Maize LAZY1 mediates shoot gravitropism and inflorescence development through regulating auxin transport, auxin signaling, and light response. Plant Physiol **163:** 1306–1322

Dreveny I, Gruber K, Glieder A, Thompson A, Kratky C (2001) The hydroxynitrile lyase from almond: a lyase that looks like an oxidoreductase. Structure **9:** 803–815

Goldberg RB, Beals TP, Sanders PM (1993) Anther development: basic principles and practical applications. Plant Cell **5:** 1217–1229

Goldberg RB, Sanders PM, Beals TP (1995) A novel cell-ablation strategy for studying plant development. Philos Trans R Soc Lond B Biol Sci **350:** 5–17

Golubovskaya IN, Hamant O, Timofejeva L, Wang CJ, Braun D, Meeley R, Cande WZ (2006) Alleles of *afd1* dissect REC8 functions during meiotic prophase I. J Cell Sci **119:** 3306–3315

Gu JN, Zhu J, Yu Y, Teng XD, Lou Y, Xu XF, Liu JL, Yang ZN (2014) DYT1 directly regulates the expression of TDF1 for tapetum development and pollen wall formation in *Arabidopsis*. Plant J **80:** 1005–1013

Hu L, Tan H, Liang W, Zhang D (2010) The *Post-meiotic Deficicent Anther1* (*PDA1*) gene is required for post-meiotic anther development in rice. J Genet Genomics **37:** 37–46

Ito T, Nagata N, Yoshiba Y, Ohme-Takagi M, Ma H, Shinozaki K (2007) *Arabidopsis MALE STERILITY1* encodes a PHD-type transcription factor and regulates pollen and tapetum development. Plant Cell **19:** 3549–3562

Jung KH, Han MJ, Lee DY, Lee YS, Schreiber L, Franke R, Faust A, Yephremov A, Saedler H, Kim YW, et al (2006) *Wax-deficient anther1* is involved in cuticle and wax production in rice anther walls and is required for pollen development. Plant Cell **18:** 3015–3032

Kim SS, Grienenberger E, Lallemand B, Colpitts CC, Kim SY, Souza CdeA, Geoffroy P, Heintz D, Krahn D, Kaiser M, et al (2010) *LAP6/POLYKETIDE SYNTHASE A* and *LAP5/POLYKETIDE SYNTHASE B* encode hydroxyalkyl α-pyrone synthases required for pollen development and sporopollenin biosynthesis in *Arabidopsis thaliana*. Plant Cell **22:** 4045–4066

Kolattukudy PE, Croteau R, Walton TJ (1975) Biosynthesis of cutin: enzymatic conversion of ω-hydroxy fatty acids to dicarboxylic acids by cell-free extracts of *Vicia faba* epidermis. Plant Physiol **55:** 875–880

Krolikowski KA, Victor JL, Wagler TN, Lolle SJ, Pruitt RE (2003) Isolation and characterization of the *Arabidopsis* organ fusion gene *HOTHEAD*. Plant J **35:** 501–511

Kunst L, Samuels AL (2003) Biosynthesis and secretion of plant cuticular wax. Prog Lipid Res **42:** 51–80

Kurdyukov S, Faust A, Trenkamp S, Bär S, Franke R, Efremova N, Tietjen K, Schreiber L, Saedler H, Yephremov A (2006) Genetic and biochemical evidence for involvement of HOTHEAD in the biosynthesis of long-chain α-,ω-dicarboxylic fatty acids and formation of extracellular matrix. Planta **224:** 315–329

Lallemand B, Erhardt M, Heitz T, Legrand M (2013) Sporopollenin biosynthetic enzymes interact and constitute a metabolon localized to the endoplasmic reticulum of tapetum cells. Plant Physiol **162:** 616–625

Li H, Pinot F, Sauveplane V, Werck-Reichhart D, Diehl P, Schreiber L, Franke R, Zhang P, Chen L, Gao Y, et al (2010) Cytochrome P450 family member CYP704B2 catalyzes the ω-hydroxylation of fatty acids and is required for anther cutin biosynthesis and pollen exine formation in rice. Plant Cell **22:** 173–190

Li J, Harper LC, Golubovskaya I, Wang CR, Weber D, Meeley RB, McElver J, Bowen B, Cande WZ, Schnable PS (2007) Functional analysis of maize RAD51 in meiosis and double-strand break repair. Genetics **176:** 1469–1482

Li N, Zhang DS, Liu HS, Yin CS, Li XX, Liang WQ, Yuan Z, Xu B, Chu HW, Wang J, et al (2006) The rice *tapetum degeneration retardation* gene is required for tapetum degradation and anther development. Plant Cell **18:** 2999–3014

Liu HL, Yin ZJ, Xiao L, Xu YN, Qu Q (2012) Identification and evaluation of ω-3 fatty acid desaturase genes for hyperfortifying α-linolenic acid in transgenic rice seed. J Exp Bot **63:** 3279–3287

Ma H (2005) Molecular genetic analyses of microsporogenesis and microgametogenesis in flowering plants. Annu Rev Plant Biol **56:** 393–434

Martin M (2011) Cutadapt removes adapter sequences from high-throughput sequencing reads. EMBnet J **17:** 10–12

Moon J, Skibbe D, Timofejeva L, Wang CJ, Kelliher T, Kremling K, Walbot V, Cande WZ (2013) Regulation of cell divisions and differentiation by MALE STERILITY32 is required for anther development in maize. Plant J **76:** 592–602

Niu BX, He FR, He M, Ren D, Chen LT, Liu YG (2013) The ATP-binding cassette transporter OsABCG15 is required for anther development and pollen fertility in rice. J Integr Plant Biol **55:** 710–720

O'Hara P, Slabas AR, Fawcett T (2001) Fatty acid synthesis in developing leaves of Brassica napus in relation to leaf growth and changes in activity of 3-oxoacyl-ACP reductase. FEBS Lett **488:** 18–22

Pawlowski WP, Wang CJ, Golubovskaya IN, Szymaniak JM, Shi L, Hamant O, Zhu T, Harper L, Sheridan WF, Cande WZ (2009) Maize AMEIOTIC1 is essential for multiple early meiotic processes and likely required for the initiation of meiosis. Proc Natl Acad Sci USA **106:** 3603–3608

Pollard M, Beisson F, Li Y, Ohlrogge JB (2008) Building lipid barriers: biosynthesis of cutin and suberin. Trends Plant Sci **13:** 236–246

Qin P, Tu B, Wang Y, Deng L, Quilichini TD, Li T, Wang H, Ma B, Li S (2013) *ABCG15* encodes an ABC transporter protein, and is essential for post-meiotic anther and pollen exine development in rice. Plant Cell Physiol **54:** 138–154

Rhee SJ, Seo M, Jang YJ, Cho S, Lee GP (2015) Transcriptome profiling of differentially expressed genes in floral buds and flowers of male sterile and fertile lines in watermelon. BMC Genomics **16:** 914

Robinson MD, McCarthy DJ, Smyth GK (2010) edgeR: a Bioconductor package for differential expression analysis of digital gene expression data. Bioinformatics **26:** 139–140

Samuels L, Kunst L, Jetter R (2008) Sealing plant surfaces: cuticular wax formation by epidermal cells. Annu Rev Plant Biol **59:** 683–707

Shi J, Cui M, Yang L, Kim YJ, Zhang D (2015) Genetic and biochemical mechanisms of pollen wall development. Trends Plant Sci **20:** 741–753

Shi J, Tan H, Yu XH, Liu Y, Liang W, Ranathunge K, Franke RB, Schreiber L, Wang Y, Kai G, et al (2011) *Defective pollen wall* is required for anther and microspore development in rice and encodes a fatty acyl carrier protein reductase. Plant Cell **23:** 2225–2246

Skibbe DS, Schnable PS (2005) Male sterility in maize. Maydica **50:** 367–376

Stieglitz H (1977) Role of β-1,3-glucanase in postmeiotic microspore release. Dev Biol **57:** 87–97

Tester M, Langridge P (2010) Breeding technologies to increase crop production in a changing world. Science **327:** 818–822

Todd J, Post-Beittenmiller D, Jaworski JG (1999) *KCS1* encodes a fatty acid elongase 3-ketoacyl-CoA synthase affecting wax biosynthesis in Arabidopsis thaliana. Plant J **17:** 119–130

Trapnell C, Pachter L, Salzberg SL (2009) TopHat: discovering splice junctions with RNA-Seq. Bioinformatics **25:** 1105–1111

Wang A, Xia Q, Xie W, Datla R, Selvaraj G (2003) The classical Ubisch bodies carry a sporophytically produced structural protein (RAFTIN) that is essential for pollen development. Proc Natl Acad Sci USA **100:** 14487–14492

Wang CJ, Nan GL, Kelliher T, Timofejeva L, Vernoud V, Golubovskaya IN, Harper L, Egger R, Walbot V, Cande WZ (2012) Maize *multiple archesporial cells 1* (*mac1*), an ortholog of rice TDL1A, modulates cell proliferation and identity in early anther development. Development **139:** 2594–2603

Wang D, Skibbe DS, Walbot V (2013) Maize Male sterile 8 (Ms8), a putative β-1,3-galactosyltransferase, modulates cell division, expansion, and differentiation during early maize anther development. Plant Reprod **26:** 329–338

Wilson ZA, Morroll SM, Dawson J, Swarup R, Tighe PJ (2001) The *Arabidopsis MALE STERILITY1* (*MS1*) gene is a transcriptional regulator of male gametogenesis, with homology to the PHD-finger family of transcription factors. Plant J **28:** 27–39

Wongnate T, Chaiyen P (2013) The substrate oxidation mechanism of pyranose 2-oxidase and other related enzymes in the glucose-methanol-choline superfamily. FEBS J **280:** 3009–3027

Xu J, Ding Z, Vizcay-Barrena G, Shi J, Liang W, Yuan Z, Werck-Reichhart D, Schreiber L, Wilson ZA, Zhang D (2014) ABORTED MICROSPORES acts as a master regulator of pollen wall formation in *Arabidopsis*. Plant Cell **26:** 1544–1556

Xu J, Yang C, Yuan Z, Zhang D, Gondwe MY, Ding Z, Liang W, Zhang D, Wilson ZA (2010) The ABORTED MICROSPORES regulatory network is required for postmeiotic male reproductive development in *Arabidopsis thaliana*. Plant Cell **22:** 91–107

Yang C, Vizcay-Barrena G, Conner K, Wilson ZA (2007) MALE STERILITY1 is required for tapetal development and pollen wall biosynthesis. Plant Cell **19:** 3530–3548

Yang X, Wu D, Shi J, He Y, Pinot F, Grausem B, Yin C, Zhu L, Chen M, Luo Z, et al (2014) Rice CYP703A3, a cytochrome P450 hydroxylase, is essential for development of anther cuticle and pollen exine. J Integr Plant Biol **56:** 979–994

Yi B, Zeng F, Lei S, Chen Y, Yao X, Zhu Y, Wen J, Shen J, Ma C, Tu J, et al (2010) Two duplicate *CYP704B1*-homologous genes *BnMs1* and *BnMs2* are required for pollen exine formation and tapetal development in Brassica napus. Plant J **63:** 925–938

Yoo SD, Cho YH, Sheen J (2007) *Arabidopsis* mesophyll protoplasts: a versatile cell system for transient gene expression analysis. Nat Protoc **2:** 1565–1572

Zhang DS, Liang WQ, Yuan Z, Li N, Shi J, Wang J, Liu YM, Yu WJ, Zhang DB (2008) Tapetum degeneration retardation is critical for aliphatic metabolism and gene regulation during rice pollen development. Mol Plant **1:** 599–610

Zhao G, Shi J, Liang W, Xue F, Luo Q, Zhu L, Qu G, Chen M, Schreiber L, Zhang D (2015) Two ATP binding cassette G transporters, rice ATP Binding Cassette G26 and ATP Binding Cassette G15, collaboratively regulate rice male reproduction. Plant Physiol **169:** 2064–2079

Zhu L, Shi J, Zhao G, Zhang D, Liang W (2013) *Post-meiotic deficient anther1* (*PDA1*) encodes an ABC transporter required for the development of anther cuticle and pollen exine in rice. J Plant Biol **56:** 59–68